Article

Cell Host & Microbe

The *Toxoplasma* Dense Granule Proteins GRA17 and GRA23 Mediate the Movement of Small Molecules between the Host and the Parasitophorous Vacuole

Graphical Abstract

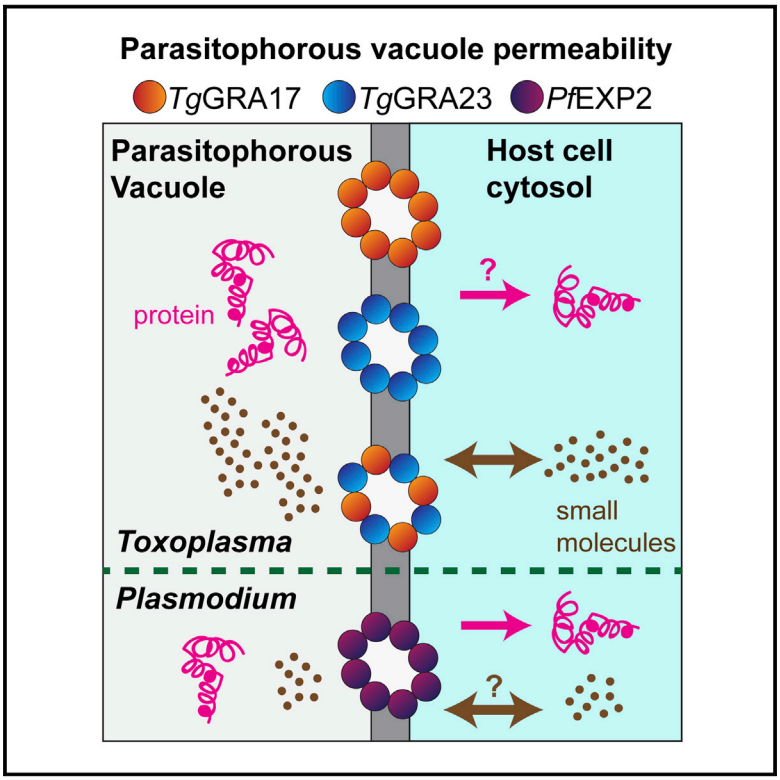

Authors

Daniel A. Gold, Aaron D. Kaplan, ..., Randall L. Rasmusson, Jeroen P.J. Saeij

Correspondence

jsaeij@mit.edu

In Brief

Toxoplasma gondii resides within an intracellular parasitophorous vacuole (PV) selectively permeable to small molecules. Gold et al. identify GRA17 and GRA23 as secreted *Toxoplasma* proteins that mediate the passage of small molecules between the host cytoplasm and PV, providing a molecular explanation for how these vacuole-residing parasites access host nutrients.

Highlights

- GRA17 and GRA23 are secreted proteins unique to PV-residing apicomplexans
- GRA17 affects the transfer of small molecules through the PV and in vivo virulence
- The GRA17 loss-of-function phenotypes can be rescued by *Plasmodium* EXP2
- GRA17 or GRA23 expression alters the membrane conductance of *Xenopus* oocytes

Gold et al., 2015, Cell Host & Microbe *17*, 642–652
May 13, 2015
http://dx.doi.org/10.1016/j.chom.2015.04.003

CellPress

Cell Host & Microbe
Article

The *Toxoplasma* Dense Granule Proteins GRA17 and GRA23 Mediate the Movement of Small Molecules between the Host and the Parasitophorous Vacuole

Daniel A. Gold,[1] Aaron D. Kaplan,[2,3] Agnieszka Lis,[2,3] Glenna C.L. Bett,[2,3,4] Emily E. Rosowski,[1] Kimberly M. Cirelli,[1] Alexandre Bougdour,[5,6] Saima M. Sidik,[7] Josh R. Beck,[8] Sebastian Lourido,[6] Pascal F. Egea,[9] Peter J. Bradley,[8] Mohamed-Ali Hakimi,[5,6] Randall L. Rasmusson,[2,3] and Jeroen P.J. Saeij[1,*]

[1]Department of Biology, Massachusetts Institute of Technology, Cambridge, MA 02139, USA
[2]Physiology and Biophysics, The State University of New York, University at Buffalo, Buffalo, NY 14214, USA
[3]Center for Cellular and Systems Electrophysiology
[4]Department of Obstetrics and Gynocology
School of Medicine & Biomedical Sciences, The State University of New York, University at Buffalo, Buffalo, NY 14214, USA
[5]UMR5163, LAPM, Centre National de la Recherche Scientifique, 38041 Grenoble, France
[6]Université Joseph Fourier, 38000 Grenoble, France
[7]Whitehead Institute for Biomedical Research, Cambridge, MA 02142, USA
[8]Department of Microbiology, Immunology and Molecular Genetics, University of California, Los Angeles, Los Angeles, CA 90095, USA
[9]Department of Biological Chemistry, UCLA David Geffen School of Medicine, Los Angeles, CA 90095, USA
*Correspondence: jsaeij@mit.edu
http://dx.doi.org/10.1016/j.chom.2015.04.003

SUMMARY

Toxoplasma gondii **is a protozoan pathogen in the phylum Apicomplexa that resides within an intracellular parasitophorous vacuole (PV) that is selectively permeable to small molecules through unidentified mechanisms. We have identified GRA17 as a *Toxoplasma*-secreted protein that localizes to the parasitophorous vacuole membrane (PVM) and mediates passive transport of small molecules across the PVM. GRA17 is related to the putative *Plasmodium* translocon protein EXP2 and conserved across PV-residing Apicomplexa. The PVs of GRA17-deficient parasites have aberrant morphology, reduced permeability to small molecules, and structural instability. GRA17-deficient parasites proliferate slowly and are avirulent in mice. These GRA17-deficient phenotypes are rescued by complementation with *Plasmodium* EXP2. GRA17 functions synergistically with a related protein, GRA23. Exogenous expression of GRA17 or GRA23 alters the membrane conductance properties of *Xenopus* oocytes in a manner consistent with a large non-selective pore. Thus, GRA17 and GRA23 provide a molecular basis for PVM permeability and nutrient access.**

INTRODUCTION

Protozoan parasites in the phylum Apicomplexa present a global human and veterinary health problem. *Toxoplasma gondii*, which causes toxoplasmosis, can infect a wide range of warm-blooded animals including humans and is a particular challenge to immune-compromised individuals such as AIDS patients and fetuses of infected mothers. Apicomplexan parasites spend the majority of their life cycle within host cells and have evolved diverse strategies to survive in this niche. Many, like *Toxoplasma* and *Plasmodium*, reside within a non-fusogenic parasitophorous vacuole (PV). The PV membrane (PVM) is the physical interface between PV-residing parasites and their host cells during intracellular growth, remaining intact until parasite egress. The PV protects parasites from being sensed by the host cell, but it is also a potential barrier to the scavenging of nutrients from the host and to parasite effectors accessing the host.

Apicomplexan parasites depend on host cells for many essential nutrients. For instance, *Toxoplasma* is auxotrophic for small molecules including amino acids like tryptophan and arginine, purines, and sterols (reviewed in Coppens, 2014). Some, like sterols, are actively scavenged from the host cell to the PV through sterol transporters on the PVM (Ehrenman et al., 2010). Transporters for small metabolites have been identified on the *Toxoplasma* plasma membrane but not on the PVM (Landfear, 2011). The *Toxoplasma*, *Plasmodium*, and *Eimeria* PVMs are selectively permeable, allowing passive, charge-independent diffusion of small molecules up to 1,300–1,900 Da into the PV, presumably through pore-like molecules on the PVM (Desai and Rosenberg, 1997; Schwab et al., 1994; Werner-Meier and Entzeroth, 1997). This is the putative mechanism by which the parasite within the PV gains access to host metabolites or effluxes toxic metabolic byproducts like lactate into the host cell. The molecular identity of the pores that grant this PVM permeability is unknown.

Toxoplasma partially circumvents the PVM barrier by secreting proteins into the host cell before and during invasion before formation of the PV from secretory organelles that include rhoptries and dense granules. Secreted effectors play a critically important role in *Toxoplasma* pathogenesis, modulating host signaling and creating a hospitable environment in the PV (reviewed in Hunter and Sibley, 2012; Kemp et al., 2013). Unlike

Table 1. *GRA17*-Like Genes Are Unique to PV-Residing Apicomplexa

Organism	GRA17-Like Genes	Gene Names	PV?
Toxoplasma gondii	2	GRA17 (TGGT1_222170), GRA23 (TGGT1_297880)	yes
Neospora caninum	2	NCLIV_005560, NCLIV_006780	yes
Hammondia hammondi	2	HHA_222170, HHA_297880	yes
Sarcocystis spp.	2	*S. neurona* A[a], *S. neurona* B; *S. muris* DG32[b]	yes
Eimeria spp.	1	*E. acervulina* EAH_00026470 (DG32) and *E. mitis* EMH_0012530 (DG32)[c]	yes
Plasmodium spp.	1	*P. falciparum* PF3D7_1471100 (EXP2), *P. knowlesi* PKH_123420 (EXP2), *P. reichenowi* PRCDC_1470300 (EXP2)	yes
Babesia bovis	0	NA	no
Cryptosporidium spp.	0	NA	no
Theileria spp.	0	NA	no
Gregarina niphandrodes	0	NA	no

The peptide sequences of GRA17 and GRA23 were used as bait in searches against apicomplexan organisms in EuPathDB.org using the BLASTP 2.0 algorithm or TBLASTN 2.2.26. Subsequent hits receiving a p value less than 0.005 were identified as similar to GRA17 and themselves used as baits in subsequent searches.

[a]The *S. neurona* genome is sequenced but unannotated, so the two *GRA17*-like genes were arbitrarily named "A" and "B."

[b]The *S. muris* genome has not been sequenced, so we cannot determine whether there is a second *GRA17*-like gene.

[c]*GRA17*-like genes were identified for all *Eimeria* and *Plasmodium* species whose genomes have been sequenced, but for brevity, only a selection of these were included in this table.

the invasion-secreted rhoptry proteins (ROPs), dense granule proteins (GRAs) are also secreted post-invasion (Karsten et al., 1998).

Plasmodium exports proteins beyond its PVM into the erythrocyte cytosol. EXP2 is the putative protein-conducting pore of the *Plasmodium* translocon for exported proteins (PTEX) complex that mediates the essential export of secreted proteins containing a *Plasmodium* export element (PEXEL) sequence motif (de Koning-Ward et al., 2009). There are also PEXEL-independent mechanisms of protein export (Grüring et al., 2012; Siau et al., 2014) that utilize the same PTEX machinery (Beck et al., 2014; Elsworth et al., 2014). In *Toxoplasma*, post-invasion protein export into the host cell has only been reported for GRA16 and GRA24 (Bougdour et al., 2013; Braun et al., 2013). Most characterized *Toxoplasma* GRA proteins are involved in organizing the structure and environment of the PV or associated with the PVM, but others such as GRA15, GRA16, and GRA24 play a role in modulating host cell signaling, suggesting that there may be more GRA proteins trafficked beyond the PVM after invasion (Bougdour et al., 2013; Mercier et al., 2005; Rosowski et al., 2011).

We sought to investigate the molecular interaction between the *Toxoplasma* PV and the host cell by studying a PVM-localized GRA protein with homology to *Plasmodium* EXP2.

RESULTS

GRA17 Is a Secreted GRA Protein Required for Normal PV Morphology

Since EXP2 has been implicated in forming a molecular-translocation channel in the *P. falciparum* PVM, we searched for homologs in the *Toxoplasma* genome and found two genes encoding proteins with predicted signal peptides: the uncharacterized *TGGT1_222170* and *TgGRA23* (*TGGT1_297880*), an identified GRA gene of unknown function (Masatani et al., 2013). TGGT1_222170 and *Tg*GRA23 share 30% amino acid sequence similarity with each other and 26% and 22% similarity with *Pf*EXP2, respectively (Figure S1A). Homologs of these proteins, including *Sarcocystis muris* DG32 (Freyer et al., 1999), were identified only in Apicomplexa that replicate within a PV (Table 1). Except for *Plasmodium spp. EXP2*, none of these genes have been functionally characterized, but due to its similarity to *GRA23*, we provisionally named *TGGT1_222170*, "*GRA17*." There is only one gene similar to *TgGRA17* or *TgGRA23* found in *Eimeria spp.* and *Plasmodium spp.*, but we found two distinct homologs in the genomes of other sequenced PV-residing Apicomplexa that are grouped in the family Sarcocystidae (Table 1; Figure S1B). We found that GRA17 and GRA23 are conserved proteins with high gene transcription levels across a global range of *Toxoplasma* strains (Melo et al., 2013; Minot et al., 2012).

Besides strongly predicted α helices, *GRA17* and *GRA23* lack sequence motifs that suggest a functional role. To characterize them, we individually disrupted the *GRA17* and *GRA23* genes and we complemented the *ΔGRA17* strain with either HA-tagged *GRA17* or *Toxoplasma*-codon-optimized *P. falciparum EXP2* transgenes that we will refer to as "*ΔGRA17+GRA17-HA*" and "*ΔGRA17+PfEXP2-HA*" (Figures S2A–S2E). The *ΔGRA17* strain was also complemented with GRA23-HA-FLAG (HF) expressed from either the putative *gra23* promoter "*ΔGRA17+GRA23-HF*$_{low}$" or from the strong *gra1* promoter "*ΔGRA17+GRA23-HF*$_{high}$"; the differing expression levels in these strains were verified by western blot (Figure S2F). We infected human foreskin fibroblasts (HFFs) with tachyzoites (the fast-replicating stage of *Toxoplasma*), fixed, and analyzed the sample by deconvolution immunofluorescence (IF) microscopy. The *ΔGRA17+GRA17-HA* strain was used for many co-staining experiments as it does not express GFP, and the GRA17-HA localization was invariant across all the strains (data not shown). We observed that GRA17-HA is intra-vacuolar and is associated with the PVM and possibly the tubulo-vesicular network (TVN) based on its partial co-localization with GRA7 (a PVM and TVN marker) and

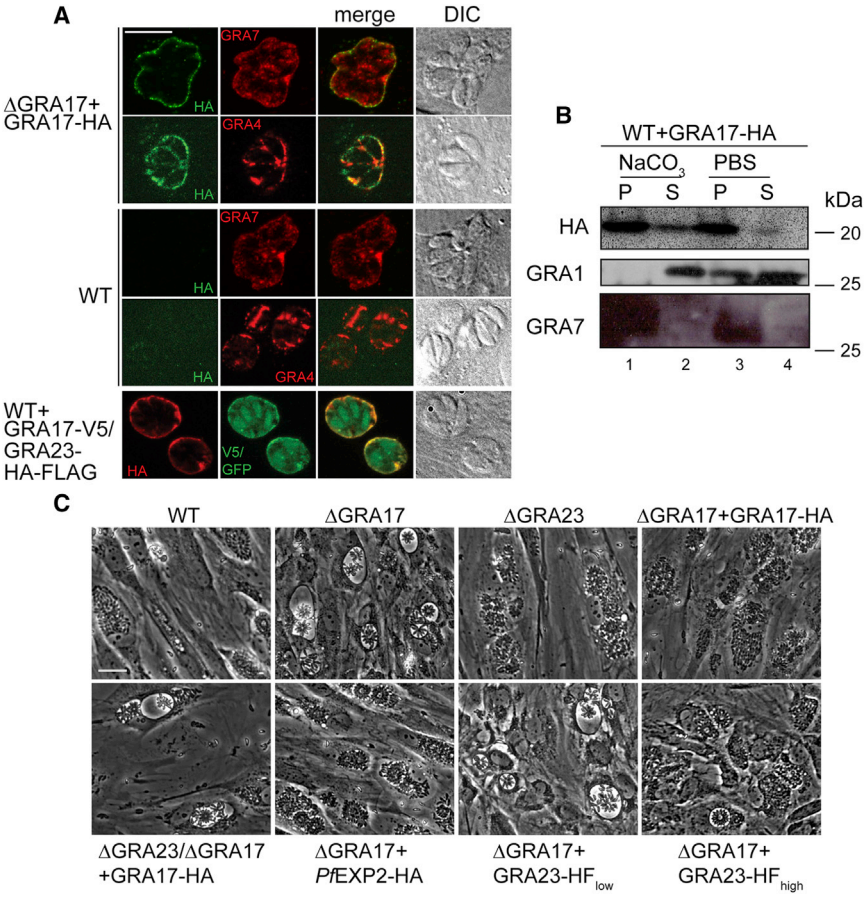

Figure 1. GRA17 Associates with the PVM and Affects PV Morphology

(A) HFFs were infected with the indicated *Toxoplasma* tachyzoite strains for 24 hr, fixed, and subjected to IF with the antibodies indicated. The WT+GRA17-V5/GRA23-HA-FLAG also expresses cytosolic GFP. The fluorescent images represent a single deconvoluted focal slice. Bright-field images were taken with differential interference contrast (DIC) microscopy (scale bar = 10 μm).

(B) HFFs were infected with WT+GRA17-HA tachyzoites for 24 hr and mechanically lysed, and a membrane-enriched fraction was treated with either PBS or sodium carbonate, centrifuged to obtain pelleted (P) and soluble (S) fractions, and subjected to SDS-PAGE. The fractions were western blotted as indicated.

(C) HFFs were infected with the indicated strains for 36 hr and imaged live by phase contrast microscopy (scale bar = 25 μm).

GRA4 (a TVN marker) especially around the periphery of the PV (Figure 1A). GRA23 has previously been characterized as a PVM-localized GRA (Masatani et al., 2013), and to observe its relative co-localization with GRA17, we generated a strain that co-expresses GRA17-V5 and GRA23-HF (the tachyzoites express GFP) and observed substantial co-localization around the PVM (Figures 1A, bottom panel, and S2G); however, the localization of GRA17-HA appeared localized to discrete foci relative to the more continuous pattern of GRA23-HF around the PVM. *Pf*EXP2-HA localized to the PVM in the *ΔGRA17* strain, and the localization of GRA23-HF was unaffected by the absence of GRA17 in the *ΔGRA17+GRA23-HF*$_{low}$ strain (Figure S2H). We confirmed that GRA17 is a GRA by observing partial co-localization of GRA17 and GRA7 in extracellular tachyzoites (Figure S2I). We raised a specific antibody against GRA17 that detected a 19 kDa band that is absent in the *ΔGRA17* strain (Figure S3A, lanes 1–4).

We tested GRA17 association with the PVM by fractionating HFFs infected with *WT+GRA17-HA* by ultracentrifugation and extracting a membrane-enriched fraction with either PBS or sodium carbonate. Sodium carbonate treatment extracts peripherally attached proteins such as GRA1, but more tightly membrane-associated proteins like GRA7 remain in the insoluble fraction (Neudeck et al., 2002; Sibley et al., 1995). We found that in contrast to GRA1, GRA17 was only minimally extracted by sodium carbonate and that the majority remained in the insoluble fraction (Figure 1B). Thus, the majority of GRA17 is tightly associated with the PVM. A similar fractionation pattern for GRA23 has been reported (Masatani et al., 2013).

We observed that a significant portion of PVs in the *ΔGRA17* strain were grossly enlarged relative to the number of parasites in the PV, whereas the *ΔGRA23* PVs are similar to wild-type (WT) (Figure 1C). Furthermore, the *ΔGRA17*-complemented strains, *ΔGRA17+GRA17-HA* and *ΔGRA17+PfEXP2-HA*, completely rescued this aberrant morphology. We were unable to generate a *ΔGRA17/ΔGRA23* strain, but we were able to delete the *GRA23* gene from the *ΔGRA17+GRA17-HA* strain, which has low GRA17 expression (Figure S3A, lanes 2 and 8). We observed that this *ΔGRA17/ΔGRA23+GRA17-HA* strain mimics the aberrant PV morphology of the *ΔGRA17* strain (Figure 1C), providing evidence of functional overlap between *GRA17* and *GRA23*. Furthermore, the *ΔGRA17* strain complemented with high (but not lower) expression of GRA23-HF partially suppressed this phenotype, with infrequent enlarged vacuoles observed (Figure 1C).

We examined whether there were other genes involved in a compensatory role with the *ΔGRA17* strain by sequencing the total mRNA from bone-marrow-derived mouse macrophages 4 hr post-infection with WT, *ΔGRA17*, *ΔGRA23*, and *ΔGRA17+GRA17-HA* strains and mapping the sequences to the *Toxoplasma* genome. As previously observed, *GRA17* expression in the *ΔGRA17+GRA17-HA* strain was 2.5-fold less compared to WT despite its ability to functionally rescue the *ΔGRA17* strain (Figure S3B) (GEO: GSE65980). *GRA23* expression levels in the *ΔGRA17* strain were 1.8-fold increased over WT levels, and *GRA17* levels were not increased in the *ΔGRA17* strain (Figure S3B). We found five additional, uncharacterized putative signal peptide-containing proteins that were uniquely upregulated in the *ΔGRA17* strain (Table S2).

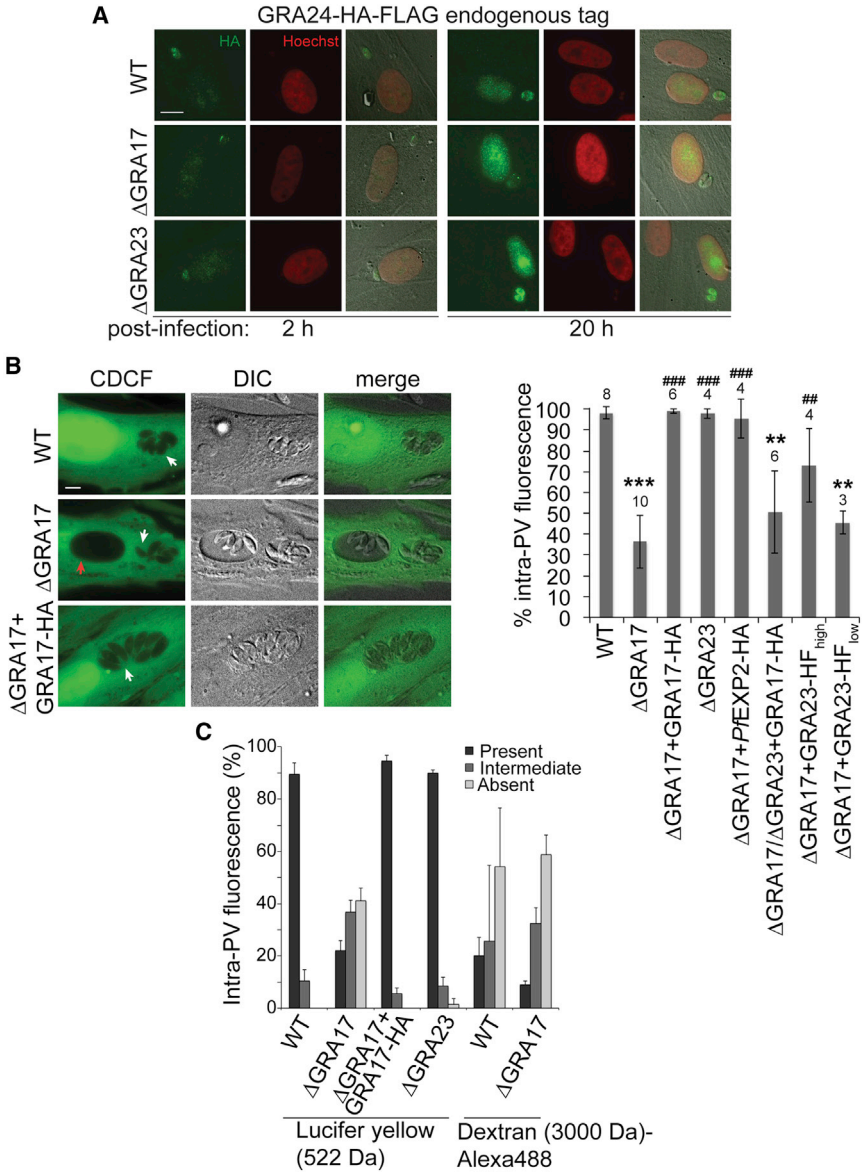

Figure 2. GRA17 Is Required for the Transfer of Small Molecules into the PV

(A) Indicated tachyzoite strains endogenously tagged with GRA24-HA-FLAG were used to infect HFFs, and the samples were fixed at the indicated time points, stained with Hoechst dye (red) and anti-HA (green), and overlaid onto a DIC image. For each channel, the exposure time is the same. This experiment was performed twice.

(B) Sub-confluent HFFs were infected with the indicated strains for 24 hr after which they were pulse labeled with CDCFDA (green) for 10 min before the cells were imaged live. White arrows indicate intra-vacuolar fluorescence and the red arrow indicates the absence of intra-vacuolar fluorescence (left panel; scale bars = 10 μm). The percentage of CDCF-fluorescent vacuoles was quantified for each strain and averaged across experiments (right panel). A minimum of 50 vacuoles per strain was counted for each replicate. Error bars represent ± SD, and the numbers above the bars of the graph indicate the number of experimental replicates for each condition. Unpaired two-tailed t tests compared to WT (***p = 3×10^{-7}; **p = 0.002) or *ΔGRA17* (### p ≤ 0.00001; ##p = 0.01) were performed.

(C) Confluent HFFs were infected with the indicated strains for 24 hr after which either lucifer yellow or Dextran3000-Alexa 488 were scrape-loaded into the cells and imaged live immediately. Intra-PV fluorescence was scored relative to the fluorescence of the individual host cell as present, intermediate, or absent as a percentage of total vacuoles (Figure S3D) and averaged across three experimental replicates (error bars are ± SD).

GRA17 Is Involved in the Movement of Small Molecules between the Host and PV

Since *Pf*EXP2 can rescue a *ΔGRA17* phenotype, we wondered whether GRA17 or GRA23 plays a role in protein export beyond the PVM. The GRA proteins GRA16 and GRA24 localize to the host nucleus with increasing intensity over the time of infection, peaking at 20 hr, indicating that they are exported across the PVM after the PV has been formed (Bougdour et al., 2013; Braun et al., 2013). We tagged the endogenous copy of GRA24 with HA-FLAG (HF) in the WT, *ΔGRA17*, and *ΔGRA23* strains. We also transiently transformed GRA16-HF into WT, *ΔGRA17*, and *ΔGRA23* extracellular tachyzoites with which we immediately infected HFFs. We then fixed the infected cells at early and late time points post-infection. Across all strains we observed a temporal increase from low to high levels of GRA16-HF and GRA24-HF staining in the host nucleus (Figures 2A and S3C). Thus, neither GRA17 nor GRA23 are individually required for GRA16 and GRA24 export beyond the PVM.

While GRA17 and GRA23 do not appear to affect protein transport across the PVM, we asked if they function as a pore for small molecules and metabolites. We used the properties of the vital dye 5-(and-6)-carboxy-2′,7′-dichlorofluorescein diacetate (CDCFDA) to test this hypothesis. CDCFDA is membrane permeable and non-fluorescent until it enters living cells, where intracellular esterases convert it into the fluorescent, membrane-impermeable 5-(and-6)-carboxy-2′,7′-dichlorofluorescein (CDCF). The molecular weight of the CDCF fluorophore (445.2 Da) is less than the established size-exclusion limit of the *Toxoplasma* PVM (Schwab et al., 1994), so we predicted that it should passively enter into the PV through the PVM but be unable to permeate through the tachyzoite plasma membrane (Schwab et al., 1994). We infected HFFs with the WT, *ΔGRA17*, *ΔGRA17+GRA17-HA*, *ΔGRA23*, *ΔGRA17+PfEXP2-HA*, *ΔGRA17/ΔGRA23+GRA17-HA*, and *ΔGRA17+GRA23-HF*$_{low/high}$ strains for 24 hr and then added a pulse of CDCFDA to the cell culture medium before washing away the dye and subsequently imaging the living cells. As predicted, we observed CDCF-fluorescence intensity equivalent to the host cytosol within nearly all the PVs of the

WT, *ΔGRA17+GRA17-HA*, *ΔGRA17+PfEXP2-HA*, and *ΔGRA23* strains but excluded from the tachyzoites themselves (Figure 2B, white arrows). By contrast, 36% of the PVs in the *ΔGRA17* strain had equivalent intra-PV CDCF-fluorescence compared to the host cytosol ($p = 4 \times 10^{-8}$ to WT; Figure 2B, red arrow and right panel), suggesting a role for GRA17 involving the passage of small molecules into the PV. We observed a similar phenotype for the *ΔGRA17/ΔGRA23+GRA17-HA* strain, with CDCF-fluorescence in 51% of PVs ($p = 0.002$ to WT and no statistical difference to *ΔGRA17*; Figure 2B, right panel). In contrast to the *ΔGRA17+GRA23-HF*$_{low}$ strain, which was similar to the *ΔGRA17* strain (45% intra-PV CDCF-fluorescence; $p = 0.002$ from WT), we observed a partial rescue of dye transfer with the *ΔGRA17+GRA23-HF*$_{high}$ strain with CDCF fluorescence in 73% of PVs that was statistically distinct from the *ΔGRA17* strain ($p = 0.01$; Figure 2B), further suggesting a synergistic role for GRA23 in small molecule permeability. Since we observed PVs of varying permeability within the same host cell (Figure 2B, *ΔGRA17*), the GRA17-mediated effect on PVM permeability to the small molecule fluorophore is PV autonomous and independent of host intracellular fluorophore concentration.

We confirmed this phenotype by introducing the membrane-impermeable dyes lucifer yellow (522 Da) or Dextran (3,000 Da)-Alexa-488 into infected cells by the technique of scrape-loading (McNeil et al., 1984). Since cellular dye uptake varies around the scrape, there was a large degree of heterogeneity of both intracellular and intra-PV dye intensities. We scored the intra-PV dye intensity relative to its host cell dye intensity as "present," "absent," or "intermediate" (Figure S3D). We found that the scrape-loaded lucifer yellow results were similar to the CDCFDA results: in contrast to >90% of WT, *ΔGRA17+GRA17-HA*, and *ΔGRA23* PVs, only 22% of *ΔGRA17* PVs were scored as having fluorescence fully equivalent to their host cells (Figure 2C). When the larger dextran (3,000 Da) dye was scrape-loaded into infected cells, we found that most of the PVs of both WT and *ΔGRA17* failed to uptake the dye, consistent with the established *Toxoplasma* PVM size-exclusion limit (Schwab et al., 1994). These results provide further evidence that *Pf*EXP2 can rescue *ΔGRA17* phenotypes and for functional overlap between GRA17 and GRA23.

The Absence of GRA17 Results in Highly Dynamic, Unstable PV

We found that fixatives altered the appearance and numbers of the enlarged, aberrant *ΔGRA17* PVs (data not shown), so we imaged the *ΔGRA17* strain live over an extended time period post-infection to observe the dynamics of these PVs. Nearly all of the PVs we observed by live imaging appeared enlarged at some point during the experimental time course. We also observed many enlarged PVs "collapsing," where the tachyzoites within them turn opaque and cease to divide. As an example, we present a multiple infected host cell where all but one PV collapses over a 5:30 hr time course (Figure 3A; Movie S1). The remaining intact PV within this cell remained enlarged and continued to divide, ultimately egressing from the cell at 62:00 hr (Movie S2). We have also observed PV collapse in singly infected cells (Figure S4A). Furthermore, we observed dynamic alteration of the size and shape of the vacuoles as exemplified by a PV that becomes grossly enlarged to the size of the entire host cell before ultimately egressing (Figure S4B; Movies S3 and S4). Since the tachyzoites within these enlarged PVs divide normally and we regularly observe egress, it indicates that they are viable.

In concordance with the PV collapse, we observed that *ΔGRA17* tachyzoites grew more slowly than WT tachyzoites. We measured this effect by quantifying the mean area of plaques formed in HFF monolayers by infection with the *ΔGRA17* and *ΔGRA23* strains relative to WT. These assays measure the overall growth of the parasites in vitro. We found that *ΔGRA17* formed plaques that were 53% the size of the WT strain ($p < 0.0001$; Figures 3B and S5A), and the *ΔGRA17+GRA17-HA* strain fully rescued this growth defect. The *ΔGRA23* strain formed plaques that were slightly smaller than the WT strain, but this effect was not significant ($p = 0.21$; Figures 3B and S5A). In contrast to the smaller plaques made by the *ΔGRA17* strain, we observed that a strain that overexpresses GRA17-HA (WT+GRA17-HA; Figure S3A, lanes 9 and 10) formed plaques that were 67% larger than WT ($p < 0.0001$; Figures 3B and S5A), implying that excess GRA17 can accelerate growth of the parasite. The collapsed PVs with non-dividing tachyzoites suggest a basis for the slow growth of the *ΔGRA17* strain in vitro.

GRA17 and GRA23 Affect the In Vivo Growth and Virulence of *Toxoplasma*

We examined whether the effects of GRA17 on overall *Toxoplasma* proliferation in vitro would manifest in vivo. We infected CD-1 outbred mice intraperitoneally (i.p.) with 100 tachyzoites of the WT, *ΔGRA17*, *ΔGRA17+GRA17-HA*, and *ΔGRA23* strains. We also infected an additional cohort with 1,000 tachyzoites of the *ΔGRA17* strain. None of the mice infected with the WT, *ΔGRA23*, and *ΔGRA17+GRA17-HA* strains survived beyond 12 days post-infection (Figure 4A), consistent with the reported hyper-virulence of the type I genetic background of our strains ($LD_{100} = \sim 1$ tachyzoite). By contrast, all of the mice infected with either the low or high dose of the *ΔGRA17* tachyzoites survived. All of these mice were seropositive and were resistant to subsequent challenge with 10,000 WT (type I) tachyzoites (Figure 4A, arrow). Subsequently, we infected cohorts of CD-1 mice with 100 tachyzoites each of the *ΔGRA17*, *ΔGRA17+GRA17-HA*, *ΔGRA17+PfEXP2-HA*, and *ΔGRA17/ΔGRA23+GRA17-HA* strains and monitored both body weight and survival. We found that none of the mice infected with *ΔGRA17+GRA17-HA* or *ΔGRA17+PfEXP2-HA* survived past 12 days post-infection, whereas all of the mice infected with the *ΔGRA17* or *ΔGRA17/ΔGRA23+GRA17-HA* strains survived the duration of the experiment (Figure 4B, top). In contrast to the mice infected with *ΔGRA17* parasites, those infected with *ΔGRA17/ΔGRA23+GRA17-HA* experienced a significant drop in body weight and deterioration in body condition (e.g., hunched stance and ruffled fur) during the course of infection before recovering fully by 30 days post-infection (Figure 4B, bottom). Thus, *Pf*EXP2 can rescue the loss of GRA17 in vivo, and the deletion of GRA23 with low GRA17 expression renders *Toxoplasma* avirulent. Since the type I strain is hyper-virulent in mice, we tested the accelerated growth in vivo by overexpressing GRA17 in the far less virulent type III strain ($LD_{50} = 10^5$ tachyzoites), which also

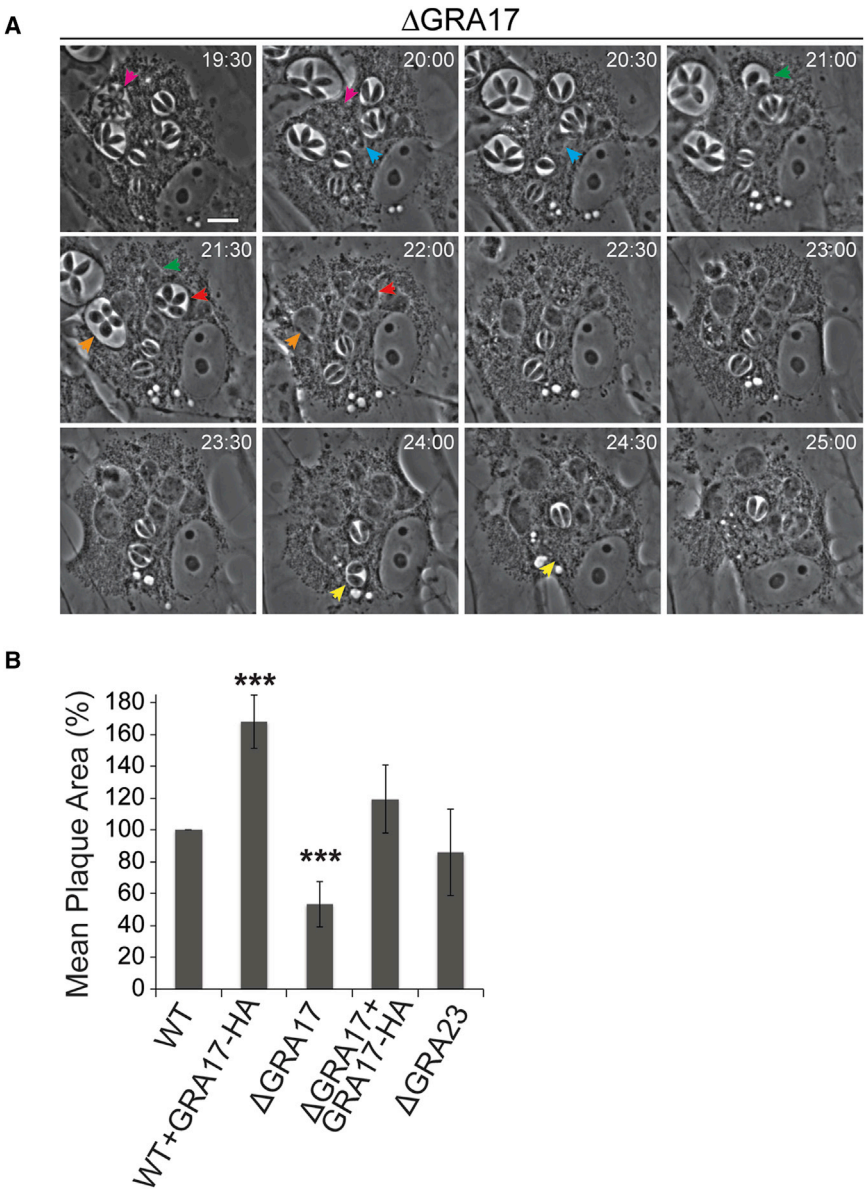

Figure 3. GRA17 Affects the Stability of *Toxoplasma* PVs

(A) Sub-confluent HFFs were infected with *ΔGRA17* tachyzoites and imaged live. Images obtained by phase contrast microscopy are presented at 30 min time points from 19:30 hr through 25:00 hr post-infection. Matching colored arrowheads indicate the collapse of indicated PVs in consecutive time points (scale bar = 10 μm).

(B) Confluent monolayers of HFFs were infected with 100 tachyzoites of each indicated strain for 4 days. For every experiment, the area of at least 30 plaques from each strain was measured (Figure S5A), and the mean area was normalized to WT. Each bar of the graph represents an average of means across experimental replicates (n = 8 for all conditions except for *ΔGRA17+GRA17-HA*, where n = 3). Error bars represent ± SD, and paired two-tailed t tests were performed comparing each condition to WT to assess statistical significance (*** $p < 0.0001$).

accelerated its in vitro growth (Figure S5B). We infected BALB/c mice with this strain and a WT (type III) strain. We found that all the infected mice survived, but the mice infected with type III+GRA17-HA had a higher parasite burden (Figure S5C), lost more weight (Figure S5D), had a worse body condition (e.g., hunched posture and ruffled coat), and had a higher brain tissue cyst count in some but not all of this cohort (Figure S5E).

GRA17 and GRA23 Are Synergistically Required for Growth

We were able to detect *ΔGRA23* phenotypes only in the background of significantly reduced GRA17 expression, and the overexpression of GRA23-HF in the *ΔGRA17* background was able to partially rescue *ΔGRA17* phenotypes, suggesting GRA17 and GRA23 operate synergistically. While we were able to generate multiple, independent clonal tachyzoite isolates of *ΔGRA17/ΔGRA23+GRA17-HA*, we could not generate a *ΔGRA17/ΔGRA23* strain in parallel by multiple methods. In order to determine whether a *ΔGRA17/ΔGRA23* strain is viable, we used the CRISPR gene disruption technology developed for *Toxoplasma* (Shen et al., 2014; Sidik et al., 2014). We chose target strains where GRA17-HA is the only species of GRA17 present so we could follow its fate by IF microscopy. As a test, we co-transformed the *ΔGRA17/ΔGRA23+GRA17-HA* strain with Cas9-3xFLAG, a guide RNA (gRNA) to target protospacer sequences early within the *GRA17* coding sequence as well as a double-stranded oligonucleotide donor template containing a nonsense mutation near the predicted Cas9-cleavage site. We co-transformed donor templates with our gRNAs, since our target strain background is *ΔKu80*, which eliminates non-homologous end-joining in favor of homologous recombination (Fox et al., 2009). We used three different gRNA/donor template pairings, fixed at 24 hr and 48 hr, and observed these gRNAs led to similar GRA17-HA loss relative to no loss with a non-specific gRNA (Figures 5A, top panel, and S6).

After transformation of both the *ΔGRA17/ΔGRA23+GRA17-HA* and *ΔGRA17+GRA17-HA* strains with Cas9-3xFLAG, a *GRA17*-specific gRNA/donor ([residues 29–36]/donor template [Leu32stop]) and subsequent infection of HFFs, we fixed infected cells early to compare the initial loss of GRA17-HA signal in the population (24 hr) to late, when the parasites will form plaques in the host cell monolayer (120 hr). Both target strains were transformed at an equivalent rate as measured by Cas9-3xFLAG detection (~27%–28%; Figure 5B, top panel). We also found that *ΔGRA17+GRA17-HA* and

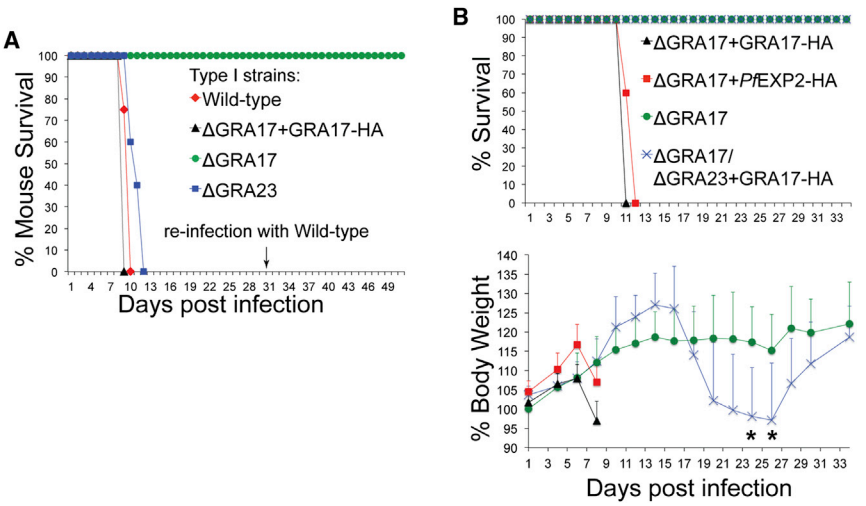

Figure 4. GRA17 Affects the Virulence and In Vivo Proliferation of *Toxoplasma*

(A) Cohorts of five female CD-1 mice (aged 6–8 weeks) were each infected with 100 tachyzoites (one additional cohort was infected with 1,000 tachyzoites of *ΔGRA17*) i.p. with each type I (RH) strain and survival was monitored. At day 30, the surviving *ΔGRA17* mice from the 100 tachyzoites infection were re-infected with 10^4 WT tachyzoites, and survival was monitored (arrow).

(B) Infection of mice was carried out as above, and survival was monitored for 34 days post-infection (top panel). The mice were weighed throughout the infection and plotted as an average of the change in body weight for each cohort, where 100% body weight is the day before infection (bottom panel). Error bars indicate +SD, and single asterisks indicate $p < 0.05$ statistical significance assessed at that time point compared to *ΔGRA17* by a Student's t test.

ΔGRA17/ΔGRA23+GRA17-HA had comparable loss of GRA17-HA signal at 24 hr post-infection (23% and 26% out of the total population, respectively; Figure 5B, top panel). By contrast, we found that 6.6% (of 584 total plaques scored) of the *ΔGRA17+GRA17-HA* plaques were GRA17-HA negative at 120 hr post-infection compared to 0% (of 934 plaques scored) in the *ΔGRA17/ΔGRA23+GRA17-HA* strain ($p < 0.0001$; Figures 5A, bottom panel, and 5B, bottom panel). In parallel, we serially diluted the transformants into HFFs to isolate tachyzoite clones: 2/20 clones from the *ΔGRA17+GRA17-HA* strain were GRA17-HA negative compared to 0/120 clones from the *ΔGRA17/ΔGRA23+GRA17-HA* strain. Taken together, our results strongly indicate that GRA17 and GRA23 are synergistically required for *Toxoplasma* growth.

GRA17 and GRA23 Alter the Membrane Conductance of *Xenopus* Oocytes

We expressed GRA17 and GRA23 in *Xenopus* oocytes to see if they can alter membrane permeability consistent with the insertion of large, relatively non-selective pores into the cell membranes. The expression of such a non-selective pore makes several experimentally testable predictions. The first is that expression will be detrimental to cells, resulting in significant cell death due to loss of cell contents and inability to maintain volume homeostasis. When varying levels of *GRA17* and *GRA23* cRNAs were injected into *Xenopus* oocytes, a dose-dependent increase in cell lysis was observed relative to water-injected cells or to *GRA15* cRNA, a GRA protein that localizes to the PVM (Rosowski et al., 2011) but which is not predicted to affect membrane permeability (Figure 6A). HA-tagged versions of GRA17, GRA23, and GRA15 were detected in total membrane fractions isolated from cRNA-injected oocytes (Figures S7A and S7B), and GRA17 and GRA23 were also observed localized to the oocyte plasma membrane in fixed histology sections (Figure S7C). The second prediction is that increased membrane permeability through expression of putative non-selective pores would cause a depolarizing shift in membrane resting potential prior to cell lysis, and GRA17 and GRA23 both demonstrated this shift relative to water- or *GRA15*-injected oocytes (Figure 6B). Finally, the current to voltage relationship of the net membrane current for a large non-selective, constitutively open pore should result in an increased linear current-voltage relationship (Figure 6C), a depolarization of the reversal potential ("V_{rev}"; Figure 6D, top panel), and an increased conductance ("G"; Figure 6D, bottom panel) for GRA17 and GRA23 relative to water- or GRA15-injected oocytes, which we observed. The results of these exogenous expression studies are strongly consistent with the hypothesis that GRA17 and GRA23 can form non-selective high-conductance pores when exogenously expressed in cell membranes. We injected a separate batch of *Xenopus* oocytes with *PfEXP2-HA* cRNA and, as with the *Toxoplasma* GRAs, found that it was present in total membrane and cytosolic fractions (Figure S7D). Relative to *GRA17* and *GRA23*, *Pf*EXP2 cRNA-injected oocytes had a more modest decrease in survival (73% compared to 93% of water-injected oocytes; Figure S7E). There was no statistically significant difference between *PfEXP2* cRNA-injected oocytes and water-injected control resting membrane potential (RMP) (Figure S7F); however, the control oocytes had a significantly depolarized RMP compared to the previous batches of oocytes used for the *Toxoplasma* GRAs (Figure 6B), making direct comparison difficult. We did observe a statistically significant increased conductance (G) change in *PfEXP2* cRNA-injected oocytes (Figures S7G and S7H), which is consistent with *Pf*EXP2 forming a large membrane pore. Further work is needed to characterize the role of *Pf*EXP2 as a membrane pore.

DISCUSSION

Intracellular pathogens that reside within vacuoles face a challenge of scavenging nutrients and modulating the host cell beyond their vacuole membrane. The existence of putative pores providing selective permeability to small molecules in the *Toxoplasma* and *Plasmodium* PVMs had been described (Desai and Rosenberg, 1997; Schwab et al., 1994), and now we have provided a molecular basis for this phenomenon in any Apicomplexa. The flow of small molecules between the host cytosol and PV plays a critical role in tachyzoite growth and survival, and its reduction may result in either restriction to nutrients or the inability of toxic metabolic byproducts to efflux

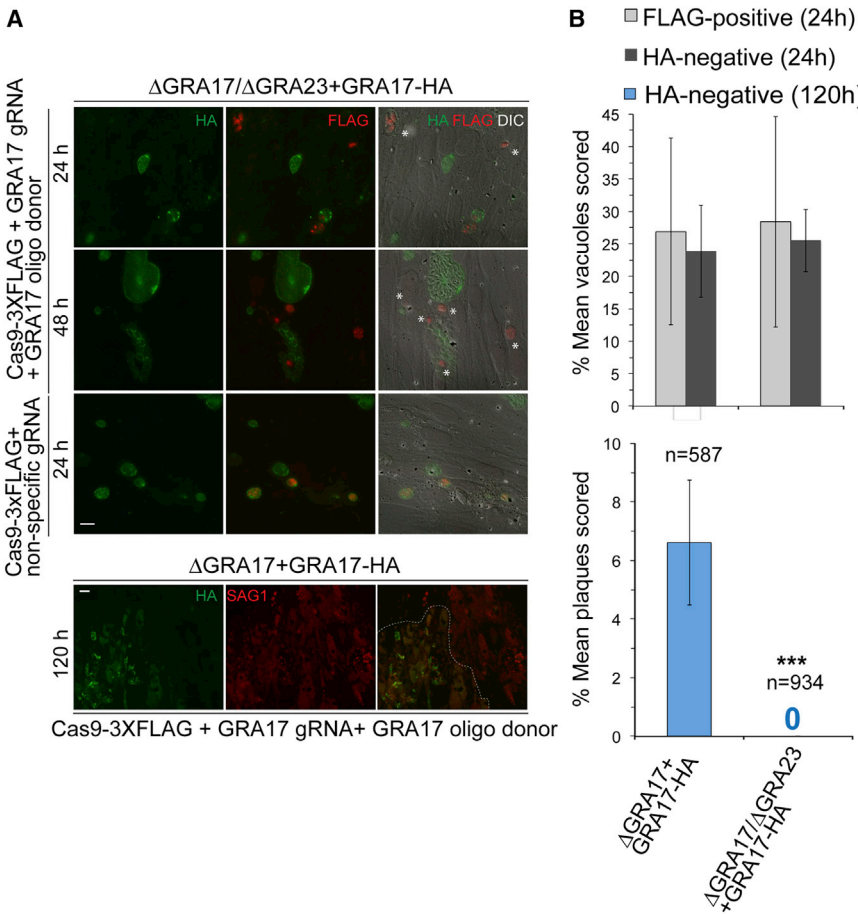

Figure 5. GRA17 and GRA23 Are Synergistically Required for Growth

(A) Confluent HFFs were infected with *ΔGRA17/ΔGRA23+GRA17-HA* or *ΔGRA17+GRA17-HA* parasites that were transiently co-transformed with Cas9-3xFLAG and either non-specific or *GRA17*-specific gRNAs along with *GRA17* donor oligonucleotide templates containing a nonsense mutation. The infected cells were fixed at 24 hr, 48 hr, or 120 hr at different MOIs and subjected to IFA with anti-HA and anti-FLAG antibodies (sample image, top left panel; scale bar = 10 μm) or anti-HA and anti-SAG1 antibodies (sample image, bottom left panel; scale bar = 25 μm). White asterisks indicate vacuoles where HA-signal is absent. The dashed line distinguishes between the two plaques.

(B) The percentage of Cas9-3xFLAG-positive vacuoles and GRA17-HA-positive vacuoles out of the total were scored and averaged (top). In total, 750 vacuoles each were scored across three experimental replicates. The percentage of Cas9-3xFLAG-positive plaques and GRA17-HA-positive plaques out of the total were scored and averaged (bottom panel). The number, n, over each bar graph refers to the total number of plaques scored in total for each condition across three experimental replicates. Error bars represent ± SD. Statistical significance was determined using a two-tailed Fisher's exact test comparing the total number of HA-negative vacuoles and plaques for both conditions (***$p < 0.0001$).

out of the PV. Overexpressing GRA17 leads to more rapid growth, suggesting that nutrients scavenged by *Toxoplasma* via GRA17 may be limiting factors for normal growth of the parasite.

An important question is how the *ΔGRA17* strain remains viable in vitro when it is starved from access to small molecules. A hint as to why some parasites retain viability lies in the aberrant morphology of the *ΔGRA17* PVs. The tachyzoites within the enlarged vacuoles are viable as they replicate and egress. The aberrant PVs may then be the byproduct or consequence of a compensatory mechanism for GRA17 absence. Compensation may include a change in the osmolarity or other structural forces, resulting in PV enlargement. The collapsed PVs may be due to ineffective compensation to reduced access to small molecules or to overcompensation that leads to PV damage. PV collapse, as well as the sensitivity of the enlarged PVs to fixatives, hints at the dynamism and fragility of the *ΔGRA17* PVs and implies a precarious balance of compensatory forces.

A prime candidate for a compensatory molecule is GRA23 based on the body of evidence we have presented. One model is that GRA17 and GRA23 may form a variety of homo- or hetero-multimers whose biophysical properties may differ depending on the composition of the complex. Alternatively, GRA17 and GRA23 may function on the PVM separately, as monomers or otherwise, having partially overlapping but ultimately separable functions. GRA17 and GRA23 may function similarly to α-helical pore-forming molecules like colicins or the pro-apoptotic protein Bax that can exist in either a water-soluble state or as an integral membrane pore that alters permeability (reviewed in Parker and Feil, 2005). Particularly intriguing are Bax-derived small α-helical peptides that can homo-multimerize within the membrane via a toroidal mechanism that does not require direct protein-protein interactions but instead contains proteins interspersed with lipids (García-Sáez et al., 2006; Qian et al., 2008). We have immunoprecipitated both GRA17 and GRA23 from PVM-containing fractions in the cell (data not shown), but we have so far not been able to identify specific interacting proteins. Our mRNA sequencing experiment did identify several other genes encoding putatively secreted protein products that are uniquely upregulated in the *ΔGRA17* strain, but none of these have been functionally characterized to date. Thus, future work is required to define the exact molecular functions of GRA17 and GRA23 as well as identify associated molecular factors.

The observation that *Plasmodium* EXP2 can rescue *ΔGRA17* phenotypes hints at a possible role of GRA17 or GRA23 in protein export in *Toxoplasma*. However, GRA16 and GRA24 accumulation in the host nucleus via post-invasion in both the *ΔGRA17* and *ΔGRA23* strains argues against such a role, although GRA17 and GRA23 may have redundant functions in protein export. It will be difficult to distinguish between a potential defect in export in the absence of both proteins versus

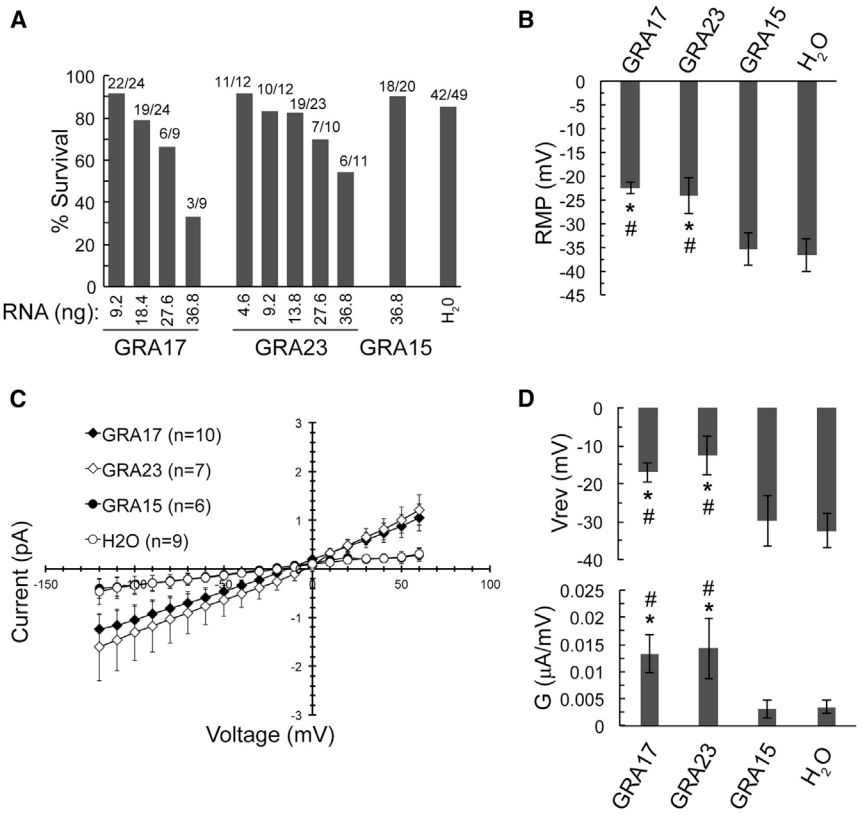

Figure 6. GRA17 or GRA23 Alter the Membrane Conductance Properties of *Xenopus* Oocytes

(A) Percentage survival of *Xenopus laevis* oocytes injected with indicated amounts of mRNA or H_2O in a dose-dependent manner 3 days post-injection. Survival was based on a morphological appearance of the oocytes. Fractions on top of each bar graph represent the number of oocytes that survived out of the total injected.

(B) Average RMPs of surviving oocytes.

(C) Average membrane currents measured from a holding potential of −90 mV potentials of −120 mV to +50 mV were applied for 2 s. Peak currents from each applied voltage were used to generate an I-V relationship.

(D) Average conductance (G, bottom) and the reversal potential (Vrev, top) were computed by fitting the I-V relationship as a straight line. For all above sub-figures, data are shown as the mean ± SE. Confidence levels were calculated using Student's paired t test, where * signifies $p < 0.05$ when compared to H_2O-injected oocytes and # signifies $p < 0.05$ when compared to GRA15-injected oocytes.

parasites that are dead or dying and thus unable to actively export protein. Ultimately, very little is known about *Toxoplasma* protein export, and there are currently only two reported exported proteins to test as candidates. Even though *Plasmodium* EXP2 has not been formally shown to be the translocation pore for protein export, it begs the question of whether it serves a dual role of nutrient pore and protein channel, since EXP2 is the only GRA17-like protein in *Plasmodium spp.* The aforementioned α-helical pore-forming proteins can form pores big enough for peptides in many cases (Parker and Feil, 2005), suggesting this dual functionality is feasible. It is possible that the other proteins in the PTEX complex may direct the function of EXP2 from a potential nutrient pore toward a role in protein export.

GRA17 and GRA23 may help elucidate another longstanding question of *Toxoplasma* biology concerning the sporozoite, the sexually derived stage found in the oocyst. After excystation from the oocyst and invasion of the host cell, the sporozoite forms a unique vacuole (PV1) in which the sporozoite undergoes no replication and ultimately egresses from the PV1 to form a second vacuole (PV2) in the same cell where it completes its conversion to the tachyzoite stage and undergoes replication. Unlike tachyzoite PVs and PV2, the PV1 is impermeable to small molecules and devoid of a subset of GRAs typically associated with PV ultrastructure, suggesting that GRA proteins play a role in this process (Speer et al., 1995). The PV1 has a strikingly enlarged morphology similar to the *ΔGRA17* PV, and neither *GRA17* nor *GRA23* are expressed in the oocyst stage (Fritz et al., 2012), implying the possibility that their absence plays a role in the unique properties of the sporozoite PV1.

We believe GRA17 and GRA23 present exciting tools to understand the challenge of how pathogens proliferate within an intracellular vacuole, which is a phenomenon widely conserved in pathogens across evolution.

EXPERIMENTAL PROCEDURES

Reagents

5-(and-6)-carboxy-2′,7′-dichlorofluorescein diacetate (C-369) and Dextran 3000-Alexa488 (D34682) were obtained from Life Technologies and lucifer yellow CH dipotassium salt (L0144) from Sigma-Aldrich.

Parasite and Cell Culture and Plaque Size Assays

Toxoplasma tachyzoites and HFFs maintenance and plaque size assays were performed as described (Rosowski et al., 2011).

Transient Transformation and Cas9-Mediated Gene Disruption

DNA sequences targeting *GRA17* were cloned into the pSS013 Cas9 vector (Sidik et al., 2014) as described in Supplemental Experimental Procedures. Transient transformations of the pSS013 plasmid were performed by co-electroporating 50–100 μg of circular DNA per strain and 25 μl of pre-annealed donor template oligonucleotides (100 μM) into freshly scrape-syringe-lysed tachyzoites, as described in Supplemental Experimental Procedures, and used to infect HFFs immediately. Confluent HFFs on coverslips were infected for fixation at 24 hr, 48 hr, and 120 hr at MOIs of 2, 0.5, and 0.04, respectively; fixed; and processed for IFA. For cloning purposes, transformed parasites were serially diluted into HFFs grown on 96-well plates without selection. Single-plaque wells were replica-passaged for propagation or for IFA with anti-HA antibodies to determine whether GRA17-HA was disrupted.

Microscopy of Fixed Samples

Microscopy was performed with NIS-Elements software (Nikon) and a digital camera (CoolSNAP EZ; Roper Scientific) connected to an inverted fluorescence microscope (eclipse Ti-S; Nikon) and either phase contrast or DIC

imaging. Deconvolution imaging was performed using the OptiGrid Structured Light Imaging System (QIOPTIQ Imaging Solutions).

Cell Fractionation

Membrane enriched fractions of infected HFFs were obtained by mechanical lysis and differential centrifugation and treated with 0.1 M sodium carbonate (pH 11) or PBS as described (Sibley et al., 1995). The resulting pellet and supernatant were subjected to SDS-PAGE and western blotting.

Live Microscopy

HFFs were grown on glass-bottom 24-well plates (Greiner Bio-One) and infected with tachyzoites for 24 hr in growth media. The cells were washed with PBS and replaced with growth media minus phenol red (GMPR) supplemented with 10 μM CDCFDA for 10 min at 37°C. CDCFDA was sequentially diluted into GMPR from a 10 mM DMSO solution. The dye-containing media was removed, and the cells were washed three times with PBS, replaced with GMPR, and were immediately imaged. Scrape-loading experiments were modified from el-Fouly et al. (1987). Briefly, infected cells were prepared as above on glass bottom 24-well plates. Either 0.5 μM lucifer yellow CH or 0.5 μg/ml Dextran3000-Alexa488 were diluted in GMPR and incubated for 5 min at 37°C. The disposable tip of a 10 μl pipette was used to scape a criss-crossed series of straight lines on the bottom of the well. The cells were washed three times with PBS, replaced with GMPR, and were immediately imaged. For the extended time course experiments, HFFs were infected with the *ΔGRA17* strain. Cells were imaged every 30 min over a 72 hr period using a 40× objective (NA = 0.95) on a Nikon TE2000 inverted microscope equipped with an environmental chamber, Hamamatsu ORCA-ER digital camera, and NIS Elements Imaging Software.

Mouse Survival and Physiology

For mouse infection, infected HFFs were mechanically lysed with 30G needles, washed with PBS, and centrifuged at 99 × *g* for 5 min to pellet any intact HFFs. The supernatant was subsequently centrifuged at 582 × *g* for 7 min to collect tachyzoites and then diluted in PBS and counted. For the survival assays, 5 female CD-1 mice (age 6–8 weeks, Charles River Laboratories) were infected i.p. with 100 tachyzoites per each strain (plus a cohort of mice was infected with 1,000 tachyzoites of *ΔGRA17*). Surviving mice were re-infected i.p. at day 30 post-infection with 10,000 tachyzoites of WT and monitored for survival for an additional 21 days. For all infections, relative parasite MOI was assessed by plaque assays, and all surviving mice were verified to be seropositive for *Toxoplasma* antigen. Mice below a body condition score of 2 were euthanized and counted as dead in accordance with institutional and federal regulations. All mice were maintained in specific pathogen-free conditions. The MIT Committee on Animal Care approved all protocols (assurance number A-3125-01).

Electrophysiology

Xenopus laevis were cared for according to standards approved by the Institutional Animal Care and Use Committee of the University at Buffalo. The frogs were anesthetized in tricaine (1 g/l; Sigma). Oocytes were digested in 82.5 mM NaCl, 2 mM KCl, 1 mM $MgCl_2$, 5 HEPES (pH 7.4), 1 mg/ml collagenase, and type I (Sigma) and shaken for 1.5 to 2 hr. Oocytes (stages V–VI) were injected with <50 ng mRNA (Nanoject; Drummond Scientific). cRNA preparation is described in Supplemental Experimental Procedures. Oocytes were voltage-clamped at room temperature with a two-electrode clamp (CA-1B; Dagan). Microelectrodes (resistances: 0.5–1.5 MΩ) were fabricated from 1.5 mm o.d. borosilicate glass tubing (TW150-4; WPI) using a two-stage puller and filled with 3 M KCl. The control extracellular solution (ND96) contained (mM) 96 NaCl, 2 KCl, 1 $MgCl_2$, 1.8 $CaCl_2$, and 10 HEPES (pH 7.4). Data were digitized and analyzed using pCLAMP (Axon). Further analysis was performed using Clampfit (Axon), Excel (Microsoft), and Origin (OriginLab). Data were filtered at 2 kHz.

SUPPLEMENTAL INFORMATION

Supplemental Information includes seven figures, two tables, four movies, and Supplemental Experimental Procedures and can be found with this article online at http://dx.doi.org/10.1016/j.chom.2015.04.003.

AUTHOR CONTRIBUTIONS

D.A.G., A.D.K., R.L.R., and J.P.S. conceived and designed the experiments, analyzed data, and wrote paper. D.A.G., A.D.K., A.L., G.C.L.B., E.E.R., and K.M.C. performed experiments. J.R.B., P.F.E., P.J.B., S.M.S., and S.L. contributed reagents.

ACKNOWLEDGMENTS

Research support: D.A.G. (Knights Templar Eye Foundation), E.E.R. (predoctoral grant in the Biological Sciences [5-T32-GM007287-33] and the Cleo and Paul Schimmel Fund), and K.M.C. (NIH, F31-AI104170). D.A.G. and J.P.S. (NIH; 1R21AI114930 and 5R01-AI080621). A.D.K., A.L., G.C.L.B., and R.L.R. (NIH; R01-HL062465). J.R.B. (NIH Microbial Pathogenesis Training Grant [T32-AI07323]) and P.J.B. (NIH; R01-AI064616, R03-AI101749). P.F.E. (UCLA STMP Award and the UCLA CTSI Grant UL1TR000124). S.L. (NIH; 1-DP5-OD017892). M.A.H. and A.B. (ERC Consolidator Grant N°614880 Hosting TOXO to M.A.H.). Thanks to P. Chang, M. Krieger, M. Vander Heiden, K. Jensen, M. Melo, M. Hassan, and E. Williams (MIT) for assistance. Thanks to Paul Chang, Sejal Vyas, Monty Krieger, Matt Vander Heiden, Kirk Jensen, Mariane Melo, Musa Hassan, and Eric Williams (MIT) for their insight and assistance.

Received: September 8, 2014
Revised: February 9, 2015
Accepted: March 20, 2015
Published: May 13, 2015

REFERENCES

Beck, J.R., Muralidharan, V., Oksman, A., and Goldberg, D.E. (2014). PTEX component HSP101 mediates export of diverse malaria effectors into host erythrocytes. Nature *511*, 592–595.

Bougdour, A., Durandau, E., Brenier-Pinchart, M.-P., Ortet, P., Barakat, M., Kieffer, S., Curt-Varesano, A., Curt-Bertini, R.-L., Bastien, O., Coute, Y., et al. (2013). Host cell subversion by *Toxoplasma* GRA16, an exported dense granule protein that targets the host cell nucleus and alters gene expression. Cell Host Microbe *13*, 489–500.

Braun, L., Brenier-Pinchart, M.P., Yogavel, M., Curt-Varesano, A., Curt-Bertini, R.L., Hussain, T., Kieffer-Jaquinod, S., Coute, Y., Pelloux, H., Tardieux, I., et al. (2013). A *Toxoplasma* dense granule protein, GRA24, modulates the early immune response to infection by promoting a direct and sustained host p38 MAPK activation. J. Exp. Med. *210*, 2071–2086.

Coppens, I. (2014). Exploitation of auxotrophies and metabolic defects in *Toxoplasma* as therapeutic approaches. Int. J. Parasitol. *44*, 109–120.

de Koning-Ward, T.F., Gilson, P.R., Boddey, J.A., Rug, M., Smith, B.J., Papenfuss, A.T., Sanders, P.R., Lundie, R.J., Maier, A.G., Cowman, A.F., and Crabb, B.S. (2009). A newly discovered protein export machine in malaria parasites. Nature *459*, 945–949.

Desai, S.A., and Rosenberg, R.L. (1997). Pore size of the malaria parasite's nutrient channel. Proc. Natl. Acad. Sci. USA *94*, 2045–2049.

Ehrenman, K., Sehgal, A., Lige, B., Stedman, T.T., Joiner, K.A., and Coppens, I. (2010). Novel roles for ATP-binding cassette G transporters in lipid redistribution in *Toxoplasma*. Mol. Microbiol. *76*, 1232–1249.

el-Fouly, M.H., Trosko, J.E., and Chang, C.-C. (1987). Scrape-loading and dye transfer. A rapid and simple technique to study gap junctional intercellular communication. Exp. Cell Res. *168*, 422–430.

Elsworth, B., Matthews, K., Nie, C.Q., Kalanon, M., Charnaud, S.C., Sanders, P.R., Chisholm, S.A., Counihan, N.A., Shaw, P.J., Pino, P., et al. (2014). PTEX is an essential nexus for protein export in malaria parasites. Nature *511*, 587–591.

Fox, B.A., Ristuccia, J.G., Gigley, J.P., and Bzik, D.J. (2009). Efficient gene replacements in *Toxoplasma gondii* strains deficient for nonhomologous end joining. Eukaryot. Cell *8*, 520–529.

Freyer, B., Hansner, T., Mehlhorn, H., and Rüger, W. (1999). Characterization of a genomic region encoding the 32-kDa dense granule antigen of *Sarcocystis muris* (Apicomplexa). Parasitol. Res. *85*, 923–927.

Fritz, H.M., Buchholz, K.R., Chen, X., Durbin-Johnson, B., Rocke, D.M., Conrad, P.A., and Boothroyd, J.C. (2012). Transcriptomic analysis of *toxoplasma* development reveals many novel functions and structures specific to sporozoites and oocysts. PLoS ONE *7*, e29998.

García-Sáez, A.J., Coraiola, M., Serra, M.D., Mingarro, I., Müller, P., and Salgado, J. (2006). Peptides corresponding to helices 5 and 6 of Bax can independently form large lipid pores. FEBS J. *273*, 971–981.

Grüring, C., Heiber, A., Kruse, F., Flemming, S., Franci, G., Colombo, S.F., Fasana, E., Schoeler, H., Borgese, N., Stunnenberg, H.G., et al. (2012). Uncovering common principles in protein export of malaria parasites. Cell Host Microbe *12*, 717–729.

Hunter, C.A., and Sibley, L.D. (2012). Modulation of innate immunity by *Toxoplasma gondii* virulence effectors. Nat. Rev. Microbiol. *10*, 766–778.

Karsten, V., Qi, H., Beckers, C.J., Reddy, A., Dubremetz, J.F., Webster, P., and Joiner, K.A. (1998). The protozoan parasite *Toxoplasma gondii* targets proteins to dense granules and the vacuolar space using both conserved and unusual mechanisms. J. Cell Biol. *141*, 1323–1333.

Kemp, L.E., Yamamoto, M., and Soldati-Favre, D. (2013). Subversion of host cellular functions by the apicomplexan parasites. FEMS Microbiol. Rev. *37*, 607–631.

Landfear, S.M. (2011). Nutrient transport and pathogenesis in selected parasitic protozoa. Eukaryot. Cell *10*, 483–493.

Masatani, T., Matsuo, T., Tanaka, T., Terkawi, M.A., Lee, E.G., Goo, Y.K., Aboge, G.O., Yamagishi, J., Hayashi, K., Kameyama, K., et al. (2013). TgGRA23, a novel *Toxoplasma gondii* dense granule protein associated with the parasitophorous vacuole membrane and intravacuolar network. Parasitol. Int. *62*, 372–379.

McNeil, P.L., Murphy, R.F., Lanni, F., and Taylor, D.L. (1984). A method for incorporating macromolecules into adherent cells. J. Cell Biol. *98*, 1556–1564.

Melo, M.B., Nguyen, Q.P., Cordeiro, C., Hassan, M.A., Yang, N., McKell, R., Rosowski, E.E., Julien, L., Butty, V., Dardé, M.-L., et al. (2013). Transcriptional analysis of murine macrophages infected with different *Toxoplasma* strains identifies novel regulation of host signaling pathways. PLoS Pathog. *9*, e1003779.

Mercier, C., Adjogble, K.D., Däubener, W., and Delauw, M.F. (2005). Dense granules: are they key organelles to help understand the parasitophorous vacuole of all apicomplexa parasites? Int. J. Parasitol. *35*, 829–849.

Minot, S., Melo, M.B., Li, F., Lu, D., Niedelman, W., Levine, S.S., and Saeij, J.P.J. (2012). Admixture and recombination among *Toxoplasma gondii* lineages explain global genome diversity. Proc. Natl. Acad. Sci. USA *109*, 13458–13463.

Neudeck, A., Stachelhaus, S., Nischik, N., Striepen, B., Reichmann, G., and Fischer, H.G. (2002). Expression variance, biochemical and immunological properties of *Toxoplasma gondii* dense granule protein GRA7. Microbes Infect. *4*, 581–590.

Parker, M.W., and Feil, S.C. (2005). Pore-forming protein toxins: from structure to function. Prog. Biophys. Mol. Biol. *88*, 91–142.

Qian, S., Wang, W., Yang, L., and Huang, H.W. (2008). Structure of transmembrane pore induced by Bax-derived peptide: evidence for lipidic pores. Proc. Natl. Acad. Sci. USA *105*, 17379–17383.

Rosowski, E.E., Lu, D., Julien, L., Rodda, L., Gaiser, R.A., Jensen, K.D., and Saeij, J.P. (2011). Strain-specific activation of the NF-kappaB pathway by GRA15, a novel *Toxoplasma gondii* dense granule protein. J. Exp. Med. *208*, 195–212.

Schwab, J.C., Beckers, C.J., and Joiner, K.A. (1994). The parasitophorous vacuole membrane surrounding intracellular *Toxoplasma gondii* functions as a molecular sieve. Proc. Natl. Acad. Sci. USA *91*, 509–513.

Shen, B., Brown, K.M., Lee, T.D., and Sibley, L.D. (2014). Efficient gene disruption in diverse strains of *Toxoplasma gondii* using CRISPR/CAS9. MBio *5*, e01114–e14.

Siau, A., Huang, X., Yam, X.Y., Bob, N.S., Sun, H., Rajapakse, J.C., Renia, L., and Preiser, P.R. (2014). Identification of a new export signal in *Plasmodium yoelii*: identification of a new exportome. Cell. Microbiol. *16*, 673–686.

Sibley, L.D., Niesman, I.R., Parmley, S.F., and Cesbron-Delauw, M.F. (1995). Regulated secretion of multi-lamellar vesicles leads to formation of a tubulo-vesicular network in host-cell vacuoles occupied by Toxoplasma gondii. J. Cell Sci. *108*, 1669–1677.

Sidik, S.M., Hackett, C.G., Tran, F., Westwood, N.J., and Lourido, S. (2014). Efficient genome engineering of *Toxoplasma gondii* using CRISPR/Cas9. PLoS ONE *9*, e100450.

Speer, C.A., Tilley, M., Temple, M.E., Blixt, J.A., Dubey, J.P., and White, M.W. (1995). Sporozoites of *Toxoplasma gondii* lack dense-granule protein GRA3 and form a unique parasitophorous vacuole. Mol. Biochem. Parasitol. *75*, 75–86.

Werner-Meier, R., and Entzeroth, R. (1997). Diffusion of microinjected markers across the parasitophorous vacuole membrane in cells infected with *Eimeria nieschulzi* (Coccidia, Apicomplexa). Parasitol. Res. *83*, 611–613.

Cell Host & Microbe, Volume *17*

Supplemental Information

The *Toxoplasma* Dense Granule Proteins GRA17 and GRA23 Mediate the Movement of Small Molecules between the Host and the Parasitophorous Vacuole

Daniel A. Gold, Aaron D. Kaplan, Agnieszka Lis, Glenna C.L. Bett, Emily E. Rosowski, Kimberly M. Cirelli, Alexandre Bougdour, Saima M. Sidik, Josh R. Beck, Sebastian Lourido, Pascal F. Egea, Peter J. Bradley, Mohamed-Ali Hakimi, Randall L. Rasmusson, and Jeroen P.J. Saeij

Fig. S1

A

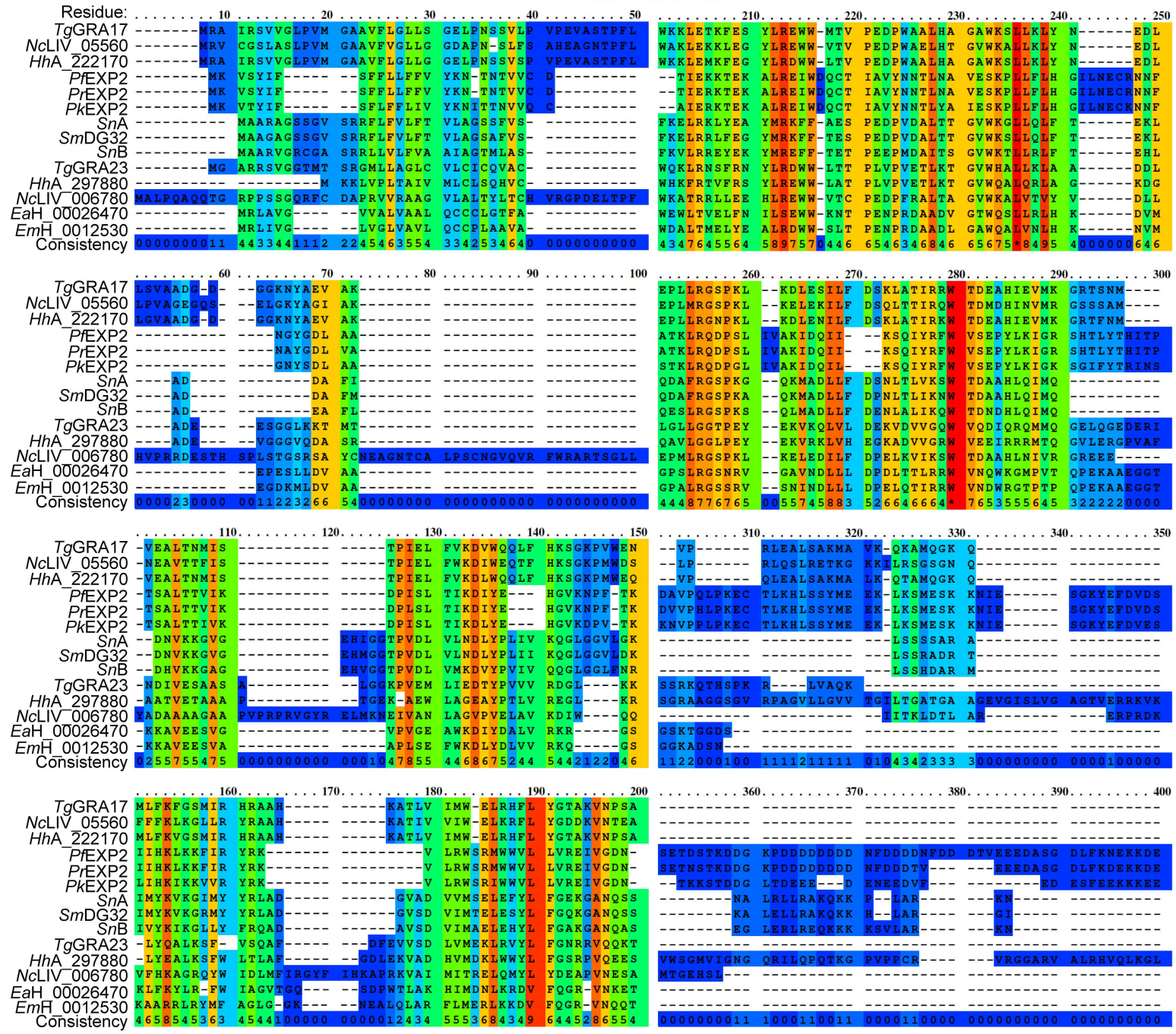
Unconserved 0 1 2 3 4 5 6 7 8 9 10 Conserved
Residue:
TgGRA17
NcLIV_05560
HhA_222170
PfEXP2
PrEXP2
PkEXP2
SnA
SmDG32
SnB
TgGRA23
HhA_297880
NcLIV_006780
EaH_00026470
EmH_0012530
Consistency

B

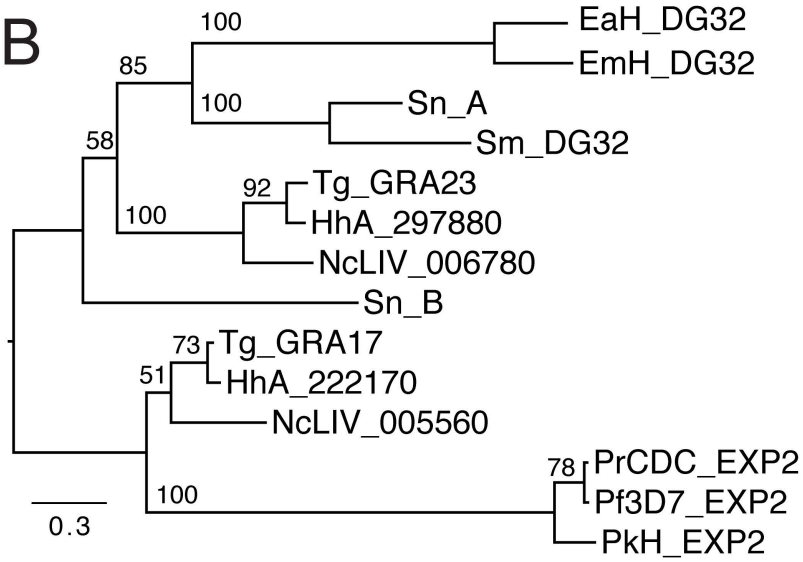
100
85
100
58
92
100
73
51
78
100
EaH_DG32
EmH_DG32
Sn_A
Sm_DG32
Tg_GRA23
HhA_297880
NcLIV_006780
Sn_B
Tg_GRA17
HhA_222170
NcLIV_005560
PrCDC_EXP2
Pf3D7_EXP2
PkH_EXP2
0.3

Fig. S2

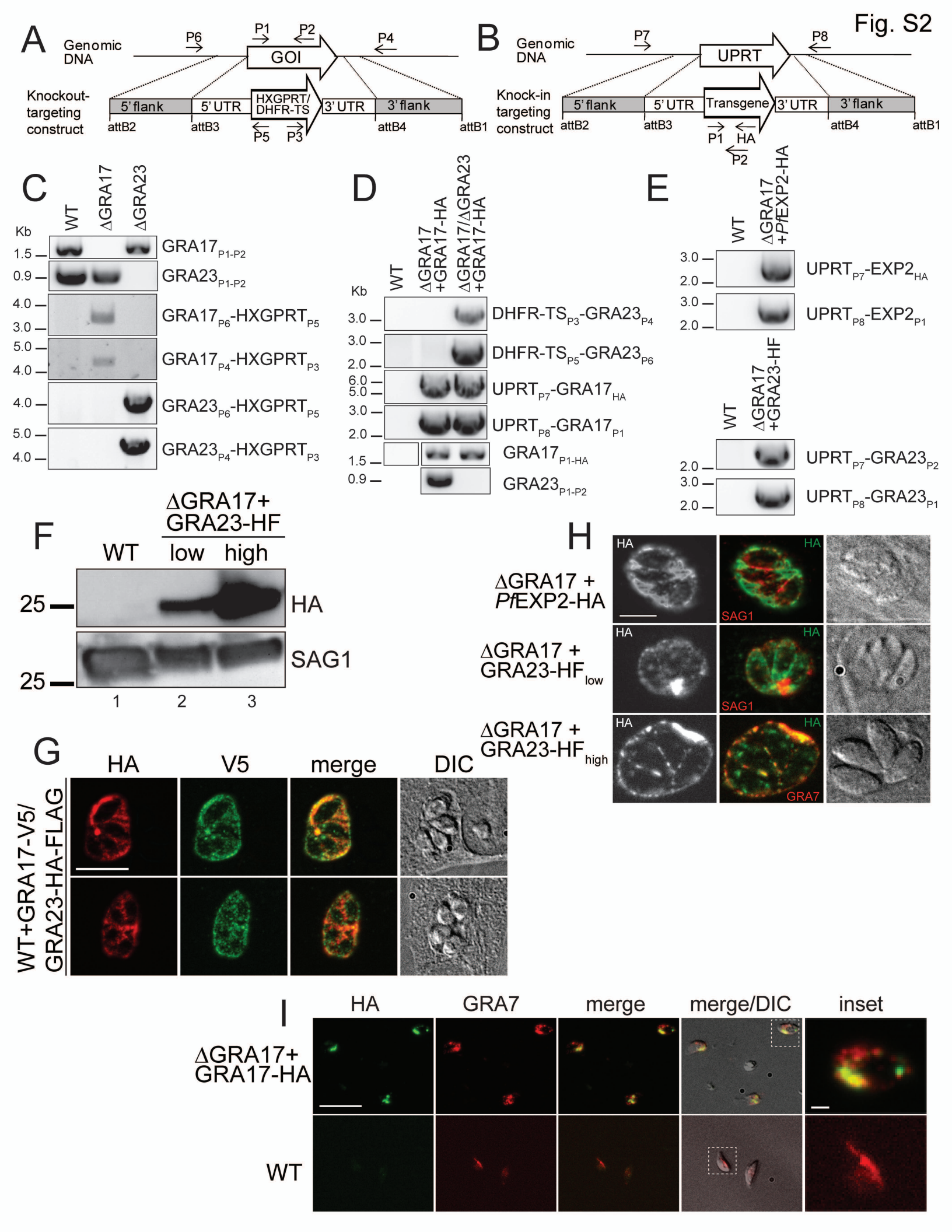
A
Genomic DNA
P6
P1
P2
GOI
P4
Knockout-targeting construct
5' flank
5' UTR
HXGPRT/ DHFR-TS
3' UTR
3' flank
attB2
attB3
P5
P3
attB4
attB1
B
Genomic DNA
P7
UPRT
P8
Knock-in targeting construct
5' flank
5' UTR
Transgene
3' UTR
3' flank
attB2
attB3
P1
HA
P2
attB4
attB1
C
WT
ΔGRA17
ΔGRA23
Kb
1.5
0.9
GRA17P1-P2
GRA23P1-P2
4.0
3.0
GRA17P6-HXGPRTP5
5.0
4.0
GRA17P4-HXGPRTP3
4.0
GRA23P6-HXGPRTP5
5.0
4.0
GRA23P4-HXGPRTP3
D
WT
ΔGRA17 +GRA17-HA
ΔGRA17/ΔGRA23 +GRA17-HA
Kb
3.0
DHFR-TSP3-GRA23P4
3.0
2.0
DHFR-TSP5-GRA23P6
6.0
5.0
UPRTP7-GRA17HA
3.0
2.0
UPRTP8-GRA17P1
1.5
GRA17P1-HA
0.9
GRA23P1-P2
E
WT
ΔGRA17 +PfEXP2-HA
3.0
2.0
UPRTP7-EXP2HA
3.0
2.0
UPRTP8-EXP2P1
WT
ΔGRA17 +GRA23-HF
2.0
UPRTP7-GRA23P2
3.0
2.0
UPRTP8-GRA23P1
F
ΔGRA17+ GRA23-HF
WT
low
high
25
HA
25
SAG1
1
2
3
G
HA
V5
merge
DIC
WT+GRA17-V5/ GRA23-HA-FLAG
H
ΔGRA17 + PfEXP2-HA
ΔGRA17 + GRA23-HFlow
ΔGRA17 + GRA23-HFhigh
HA
SAG1
GRA7
I
HA
GRA7
merge
merge/DIC
inset
ΔGRA17+ GRA17-HA
WT

Fig. S3

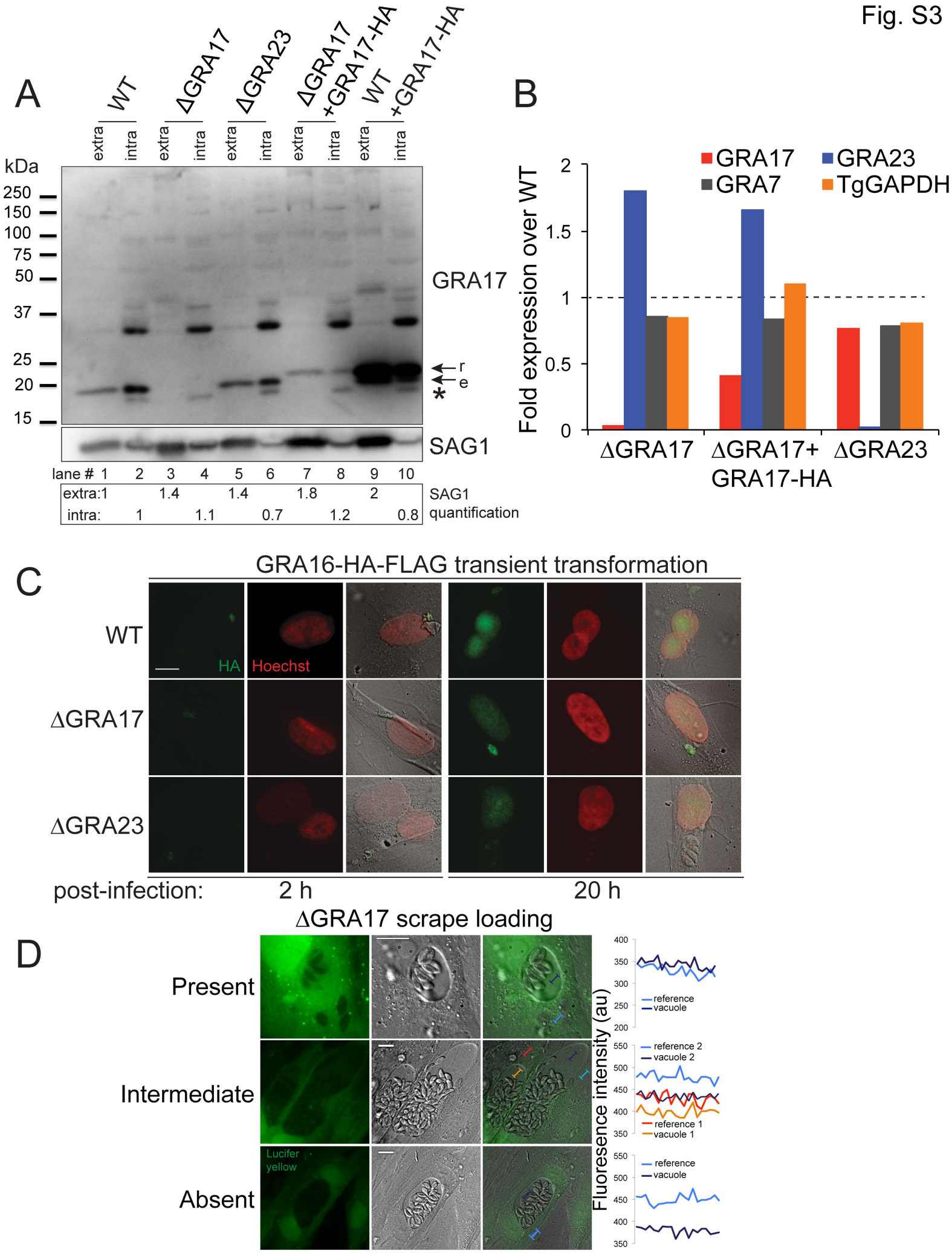
A
WT
ΔGRA17
ΔGRA23
ΔGRA17 +GRA17-HA
WT +GRA17-HA
extra
intra
kDa
250
150
100
75
50
37
25
20
15
GRA17
r
e
SAG1
lane # 1 2 3 4 5 6 7 8 9 10
extra:1 1.4 1.4 1.8 2
intra: 1 1.1 0.7 1.2 0.8
SAG1 quantification
B
GRA17
GRA23
GRA7
TgGAPDH
Fold expression over WT
2
1.5
1
0.5
0
ΔGRA17
ΔGRA17+ GRA17-HA
ΔGRA23
C
GRA16-HA-FLAG transient transformation
WT
ΔGRA17
ΔGRA23
HA
Hoechst
post-infection:
2 h
20 h
D
ΔGRA17 scrape loading
Present
Intermediate
Absent
Lucifer yellow
Fluorescence intensity (au)
reference vacuole
reference 2 vacuole 2
reference 1 vacuole 1

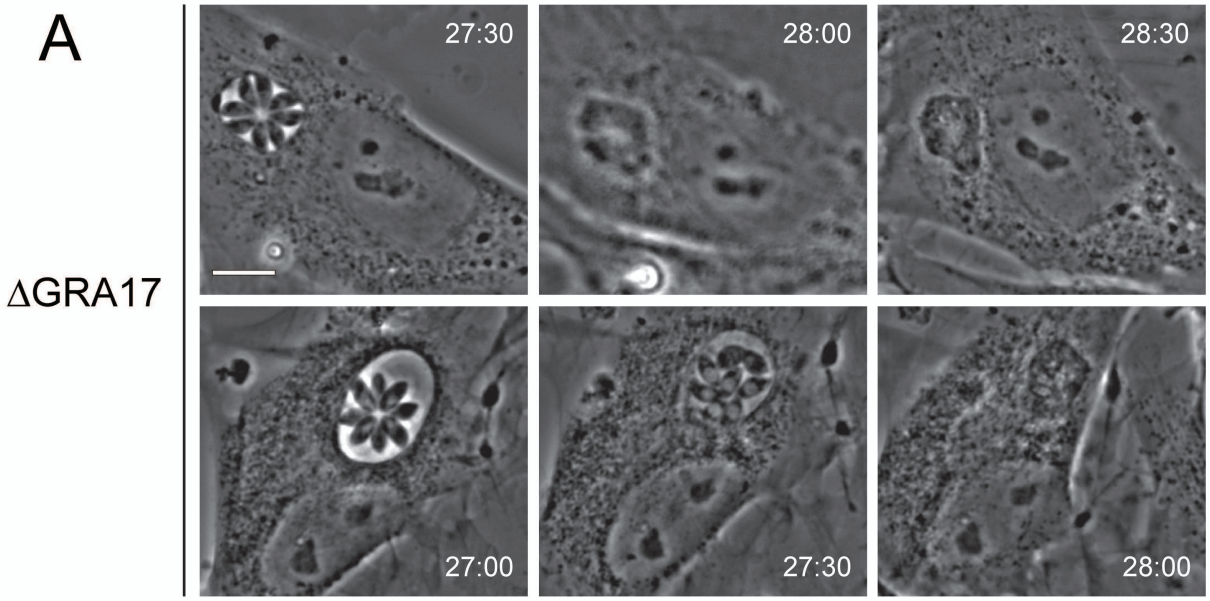
A
ΔGRA17
27:30
28:00
28:30
27:00
27:30
28:00

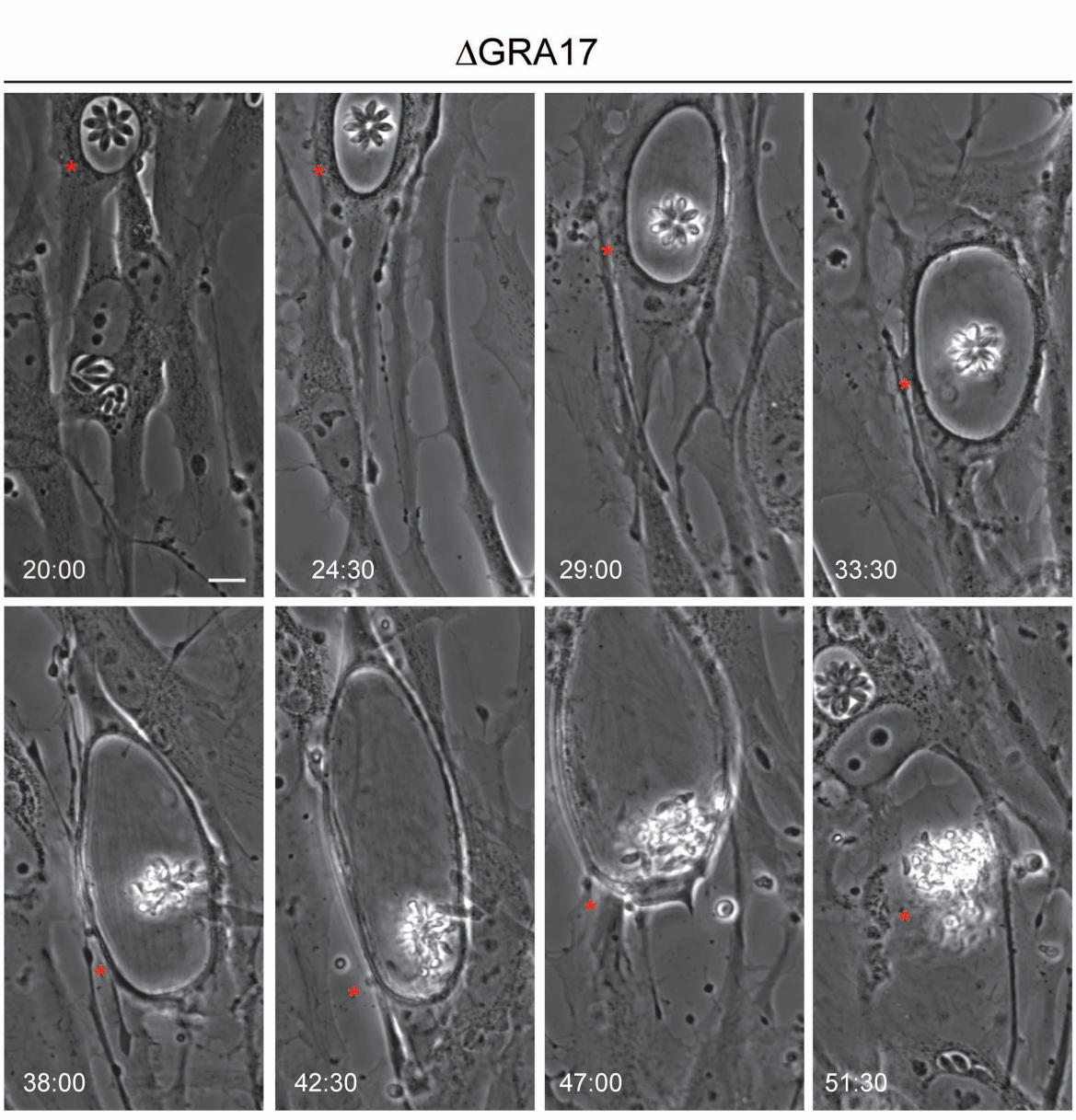
B
ΔGRA17
20:00
24:30
29:00
33:30
38:00
42:30
47:00
51:30

Fig. S5

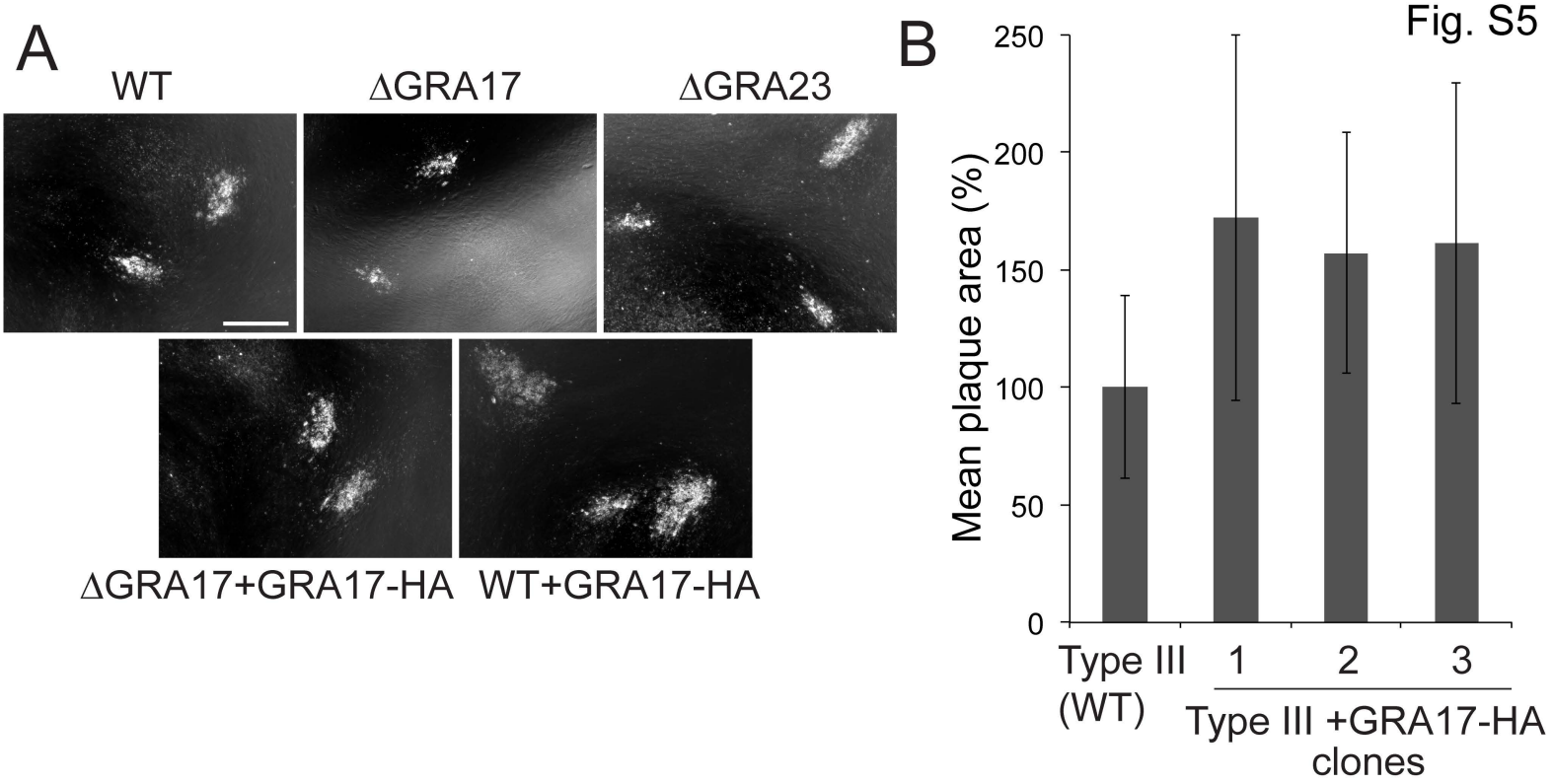
A
WT
ΔGRA17
ΔGRA23
ΔGRA17+GRA17-HA
WT+GRA17-HA
B
Mean plaque area (%)
250
200
150
100
50
0
Type III (WT)
1
2
3
Type III +GRA17-HA clones

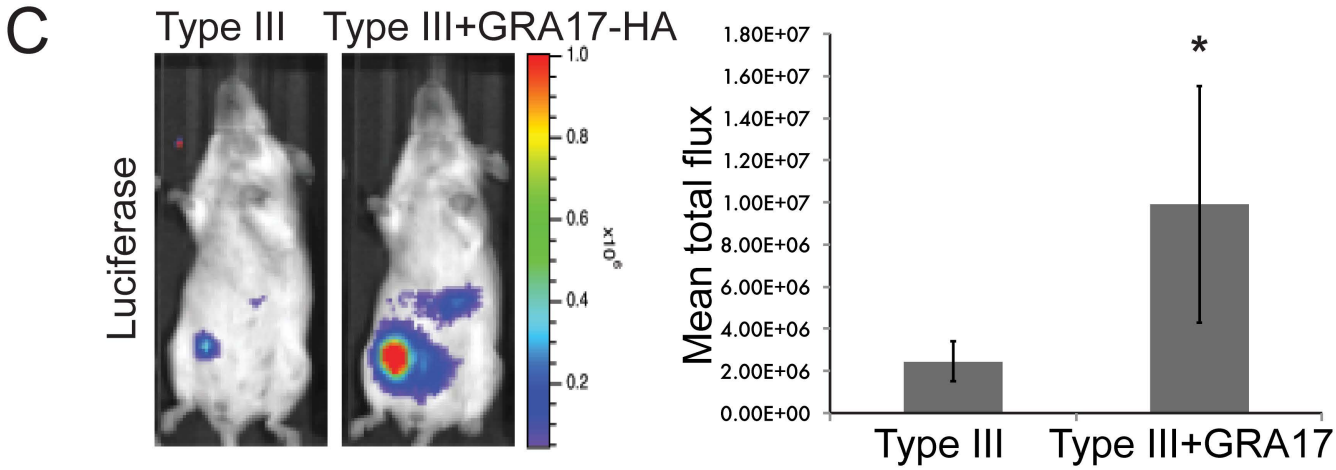
C
Type III
Type III+GRA17-HA
Luciferase
1.0
0.8
0.6
0.4
0.2
x10⁶
Mean total flux
1.80E+07
1.60E+07
1.40E+07
1.20E+07
1.00E+07
8.00E+06
6.00E+06
4.00E+06
2.00E+06
0.00E+00
*
Type III
Type III+GRA17

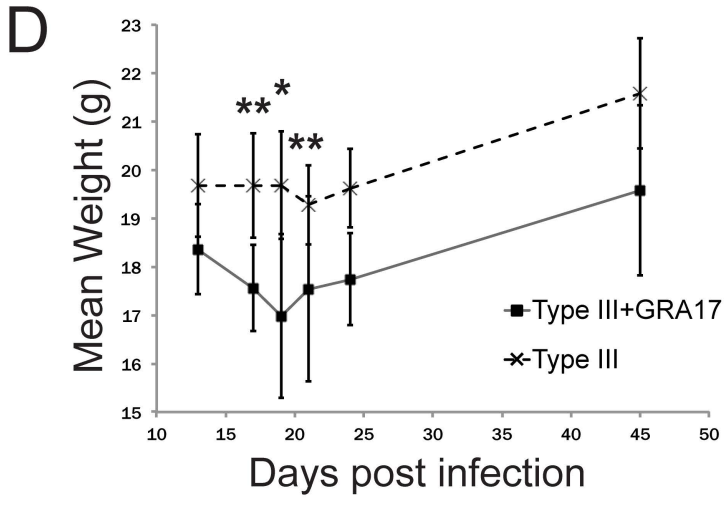
D
Mean Weight (g)
23
22
21
20
19
18
17
16
15
**
*
**
Type III+GRA17
Type III
10
15
20
25
30
35
40
45
50
Days post infection

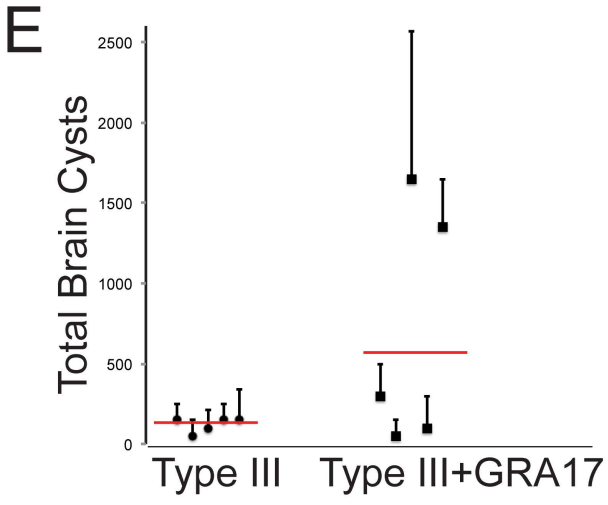
E
Total Brain Cysts
2500
2000
1500
1000
500
0
Type III
Type III+GRA17

Fig. S6

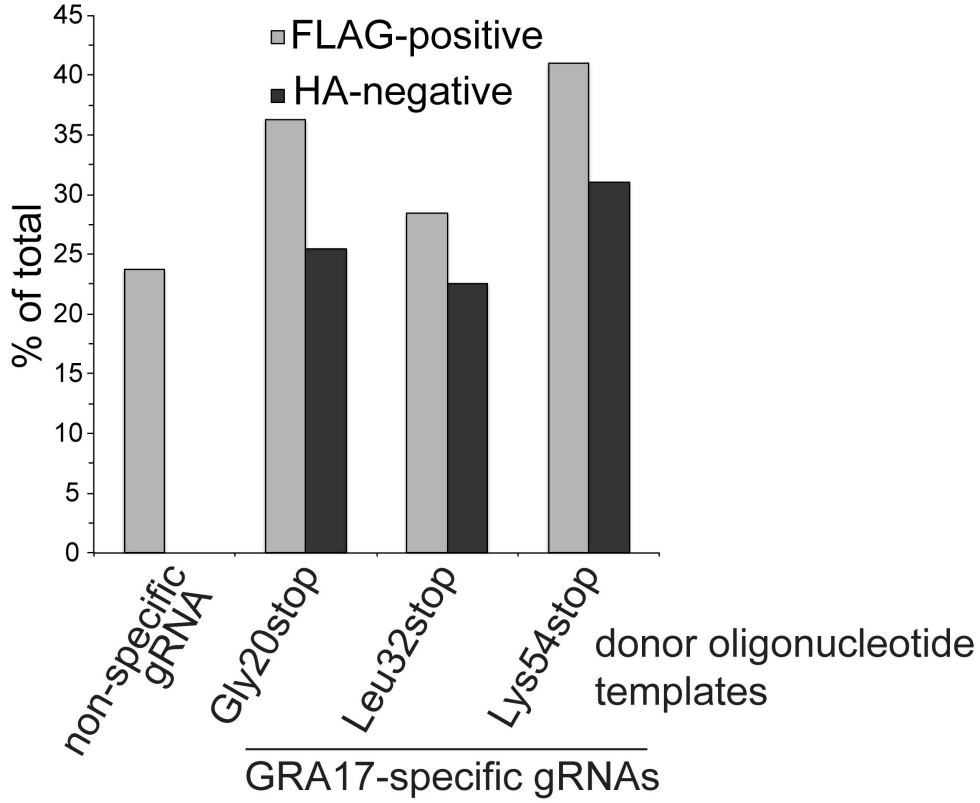
FLAG-positive
HA-negative
% of total
45
40
35
30
25
20
15
10
5
0
non-specific gRNA
Gly20stop
Leu32stop
Lys54stop
donor oligonucleotide templates
GRA17-specific gRNAs

Fig. S7

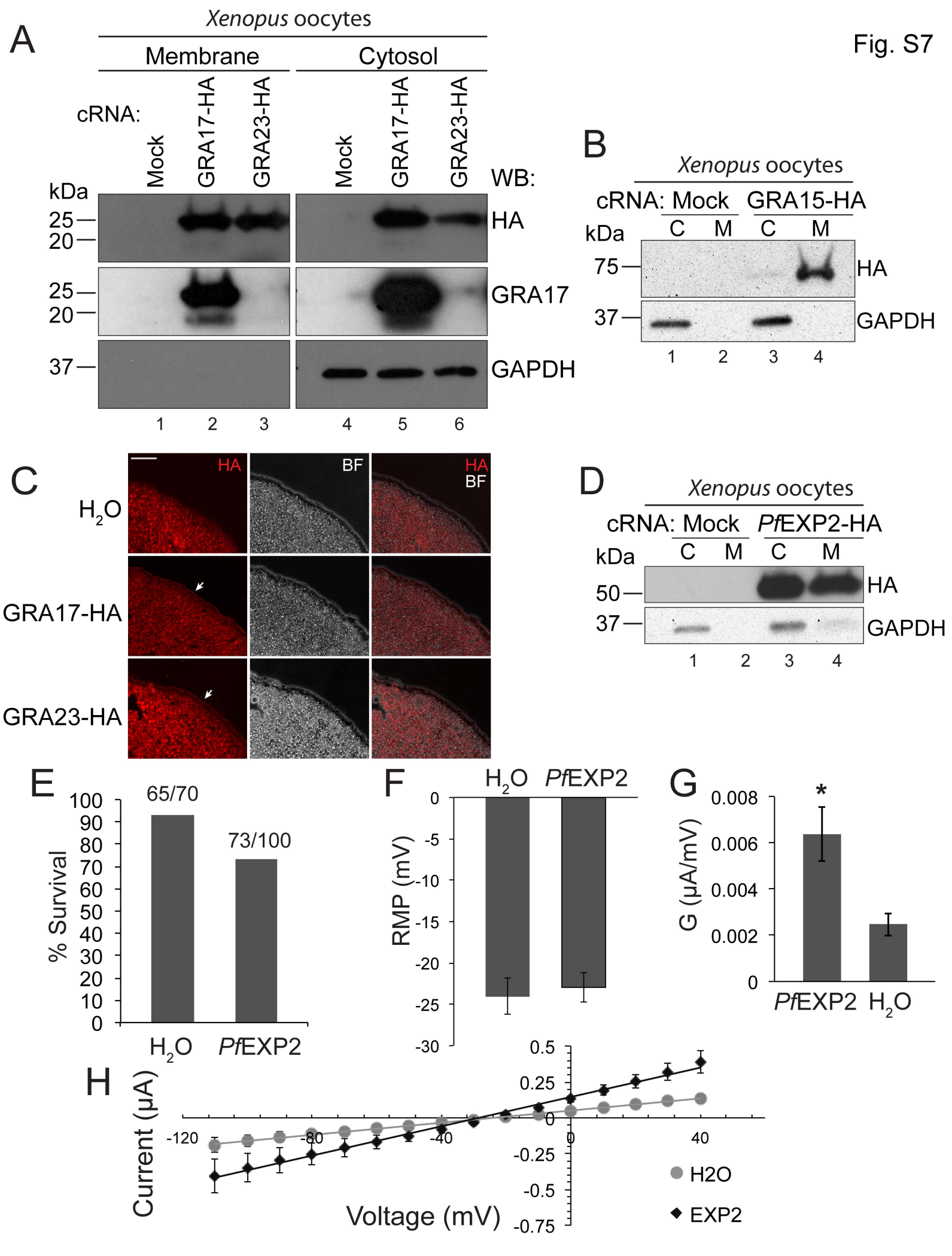
A
Xenopus oocytes
Membrane
Cytosol
cRNA:
Mock
GRA17-HA
GRA23-HA
Mock
GRA17-HA
GRA23-HA
WB:
kDa
25
20
HA
GRA17
37
GAPDH
1 2 3 4 5 6
B
Xenopus oocytes
cRNA: Mock GRA15-HA
C M C M
kDa
75
HA
37
GAPDH
1 2 3 4
C
HA
BF
HA BF
H2O
GRA17-HA
GRA23-HA
D
Xenopus oocytes
cRNA: Mock PfEXP2-HA
C M C M
kDa
50
HA
37
GAPDH
1 2 3 4
E
65/70
73/100
% Survival
H2O
PfEXP2
F
H2O PfEXP2
RMP (mV)
G
*
G (µA/mV)
PfEXP2 H2O
H
Current (µA)
Voltage (mV)
H2O
EXP2

Figure S1. Sequence alignment and analysis of GRA17, related to Table 1.

(A) Alignment of the primary peptide sequences of *Toxoplasma gondii* GRA17 (TGGT1_222170)[1] and GRA23 (TGGT1_297880), *Neospora caninum* NCLIV_005560 and NCLIV_006780, *Sarcocystis muris* DG32 (O43946_SARMU), *Sarcocytis neurona* A and B (unannotated), *Eimeria acervulina* EAH_00026470, *E. mitis* EMH_0012530 and the EXP2 genes from *Plasmodium falciparum* (PF3D7_1471100), *Plasmodium knowlesi* (PKH_123420), and *Plasmodium reichenowi* (PRCDC_1470300) using Profile ALIgNmEnt (PRALINE) (Bawono and Heringa, 2014) which scores amino acid conservation. The scoring scheme works from 0 for the least conserved alignment position, up to 10 for the most conserved alignment position. The color assignments are depicted in the legend (*above*). **(B)** The phylogenetic tree represents full-length peptide sequences from the previous alignment, using the Neighbor-Joining method with the program MEGA5 (Tamura et al., 2011). The percentage of replicate trees in which the associated taxa clustered together in the bootstrap test (500 replicates) is shown next to the branches. The tree is drawn to scale (*below*), with branch lengths in the same units as those of the evolutionary distances used to infer the phylogenetic tree. The evolutionary distances were computed using the JTT matrix-based method and are in the units of the number of amino acid substitutions per site. All positions containing gaps and missing data were eliminated.

[1] A *Toxoplasma* Kozak sequence is present immediately upstream of the second methionine (residue 58) from the predicted *GRA17* coding sequence on ToxoDB.org (v13.0) and the observed size of the GRA17 band (19 kDa; Fig. S3A) matches the signal peptidase cleavage product predicted from the *GRA17* coding sequence starting from that second methionine in contrast to the size discrepancy that exists with the current gene model on ToxoDB.org (v13.0). This suggests that Met58 (from the current gene model) is the actual *GRA17* start codon.

Figure S2. Confirmation of gene knockouts and transgenic expression, related to Figure 1.

(A) Schematic diagram depicting the genomic loci of the genes of interest (GOI) (*top*) and the gene knockout-targeting construct (pTKO2-HXGPRT or pTKO2-DHFR-TS) used to disrupt GOI loci (*bottom*). The construct consists of the *HXGPRT* or *DHFR-TS* selection cassettes flanked by UTRs derived from *TgDHFR*, which in turn is flanked by 5' and 3' targeting sequences (described in Experimental Procedures) corresponding to regions flanking the GOI coding sequences. P1 and P2 refer to primers annealing within the coding region of the GOI (either *GRA17* or *GRA23*). P3 and P5 are sense and antisense primers annealing within the *HPT* or *DHFR-TS* selection cassettes. P6 and P4 refer to sense and antisense primers annealing outside the 5' and 3' flanking sequences surrounding either the *GRA17* or *GRA23* loci. **(B)** Schematic diagram depicting the genomic locus of *TgUPRT* (*top*) and the knock-in-targeting construct (pTKO2-UPRT) containing the transgenes used to disrupt the *UPRT* loci (*bottom*). The construct encodes the transgenes and accompanying UTRs, which in turn are flanked by 5' and 3' targeting sequences (described in Experimental Procedures) corresponding to the *UPRT* loci. P1, P2, and HA are sense and antisense primers annealing within the coding region of the transgenes. P7 and P8 refer to sense and antisense primers annealing outside the 5' and 3' targeting sequences surrounding the *UPRT* locus. **(C)** The absence of PCR products amplified by P1/P2 from genomic DNA derived from the *ΔGRA17* and *ΔGRA23* strains (in contrast to WT) verify of the disruption of the GRA17 and GRA23 loci (*top two panels, respectively*). The PCRs products amplified by the P6/P5 and P3/P4 primers verify the orientation of the knockout construct within the GRA17 or GRA23 loci (*bottom four panels*). **(D)** The PCRs products amplified by the P6/P5 and P3/P4 primers from genomic DNA derived from the *ΔGRA17*/*ΔGRA23*+*GRA17-HA* strain (in contrast to WT and *ΔGRA17*+*GRA17-HA* strains) verify the orientation of the *DHFR-TS* knockout

cassette within the *GRA23* locus (*top two panels*). The PCRs products amplified by the P7/HA, P1/P8, and P1/HA primers from genomic DNA derived from the *ΔGRA17+GRA17-HA* and *ΔGRA17/ΔGRA23+GRA17-HA* strains (in contrast to WT) verify the presence and orientation of the GRA17-HA transgene within the *UPRT* locus (*third, fourth, and fifth panels from top*). The absence of a PCR product amplified by P1/P2 from genomic DNA derived from the *ΔGRA17/ΔGRA23+GRA17-HA* strain (in contrast to *ΔGRA17+GRA17-HA*) verifies the disruption of the *GRA17* locus (*bottom panel*). **(E)** The PCRs products amplified by the P7/HA and P1/P8 primers from genomic DNA derived from the *ΔGRA17+EXP2-HA* and *ΔGRA17+(gra1-5'UTR)-GRA23-HA-FLAG (HF)* strains (in contrast to WT) verify the presence and orientation of the *(gra1-5'UTR)-EXP2-HA* (*top two panels*) and *(gra1-5'UTR)-GRA23-HF$_{high}$* (*bottom two* panels) transgenes within the *UPRT* locus. **(F)** Wild-type (WT), *ΔGRA17+(gra23-5'UTR)-GRA23-HF*$_{low}$, and *ΔGRA17+(gra1-5'UTR)-GRA23-HA-FLAG*$_{high}$ extracellular parasites were lysed with sample buffer, subjected to SDS-PAGE and Western blotted with anti-HA and anti-SAG1 antibodies. **(G)** HFFs were infected with WT+GRA17-V5/GRA23-HF as in Fig. 1A except that the samples were fixed with methanol to quench GFP fluorescence and stained with anti-HA and anti-V5 antibodies as indicated (scale bar = 10 μm). **(H)** HFFs were infected for 24 h with *ΔGRA17+PfEXP2-HA*, *ΔGRA17+(gra23-5'UTR)-GRA23-HA-FLAG*$_{low}$, and *ΔGRA17+(gra1-5'UTR)-GRA23-HA-FLAG*$_{high}$ parasites, fixed and stained with anti-HA and anti-SAG1 antibodies and imaged by IF and DIC microscopy; scale bar = 5 μm. **(I)** Extracellular tachyzoites were fixed and stained with anti-HA (*red*) and anti-GRA7 (*green*) antibodies and imaged with deconvolution as above and merged with a DIC brightfield image; scale bar = 5 μm.

Figure S3. GRA17 physical and functional characterization, related to Figure 2.

(A) HFFs were infected with the indicated *Toxoplasma* strains for 24 h and lysed to obtain intracellular (intra) lysates or tachyzoites were allowed to completely egress to

obtain extracellular (extra) lysates, which were then subjected to SDS-PAGE and Western blotted with either serum raised against a C-terminal epitope of GRA17 or antibodies against *Toxoplasma* Surface Antigen (SAG)-1, used here as a loading control. The *arrows* distinguish between the epitope-tagged recombinant and endogenous forms of GRA17. The *asterisk* denotes a non-specific band found in the intracellular lysates. The designations "r" and "e" refer to the recombinant and endogenous species of GRA17, respectively. SAG1 bands were quantified by optical density and normalized to either intracellular or extracellular WT lanes as indicated. **(B)** Total mRNA was isolated and sequenced from bone marrow-derived mouse macrophages that were infected with equivalent MOI-matched wild-type, *ΔGRA17, ΔGRA17+GRA17-HA*, and *ΔGRA23*, and tachyzoites for 4 hours. The expression data is expressed as fold change of the transcript counts of the *GRA17* (*red*), *GRA23* (*blue*), *GRA7* (*charcoal*) and *T. gondii GAPDH* (*orange*) genes compared to wild-type levels (*dotted line*). This experiment was performed once. **(C)** Wild-type, *ΔGRA17*, and *ΔGRA23* tachyzoites were transiently transformed with GRA16-HA-FLAG and immediately used to infect HFFs and fixed at 2 h and 20 h post-infection and subjected to IF with anti-HA antibodies (*green*) or stained with Hoechst dye (*red*) and overlaid on a DIC image. This experiment was performed twice; scale bar = 10 μm. **(D)** Sample images of *ΔGRA17*-infected HFFs that have been scrape-loaded with Lucifer Yellow dye (*green*) alone or overlaid onto a DIC image that exemplify the intra-PV fluorescence scores as described in Fig. 2C (*left panel*). Using the NIS Elements software, fluorescence intensity (arbitrary units) was plotted across a line of defined length within the vacuole or as a reference, outside the vacuole for each example (*right panel*; scale bar = 10 μm).

Figure S4. GRA17 dynamically affects PV morphology, related to Figure 3.

(A) Sub-confluent HFFs on were infected with *ΔGRA17* tachyzoites and imaged live under identical conditions as in Fig. 3A. Images obtained from two different cells; phase-contrast microscopy from indicated time-points. **(B)** As in (A), time-points of images from one cell range from 20 h to 51:30 h post-infection when the tachyzoites egress. The *red asterisks* indicate the same PV followed over time, which along with its host cell moved out of the fixed field of view times over the experimental time course. Scale bar = 10 μm for both subfigures.

Figure S5. GRA17 affects *in vitro* and *in vivo* growth, related to Figure 4.

(A) Representative plaque images from the analysis in Fig. 3C from each strain are presented. Plaques were imaged at 4× magnification by phase-contrast microscopy taken out of phase to increase contrast; scale bar = 0.5 mm. **(B)** Confluent monolayers of HFFs in individual wells of 24-well plates were infected with 300 tachyzoites of each indicated type III strain for 7 days. The area of at least 30 plaques from each strain was measured and the mean area was normalized to wild-type (WT). This experiment was performed once. **(C)** Five female BALB/c mice were each infected with 10^4 tachyzoites intraperitoneally with the indicated strains expressing firefly luciferase and were imaged *in vivo* at 4 days post-infection. One representative of the 5 mice infected is shown (*left).* Each bar of the graph (*right*) represents a mean of the total flux (photons/sec/cm^2/sr) per mouse of each strain as an assessment of parasite burden. Error bars represent ±SD and a Student's *t* test was used to measure statistical significance (P=0.05). **(D)** The average weight of the five mice infected with each strain in (B) was plotted over time as an assessment of overall health. Error bars represent ±SD and a two-tailed Student's *t* test was used to measure statistical significance. **(E)** At 45 days post-infection, *Toxoplasma* tissue cysts were counted by staining homogenates of brains derived from each mouse with dolichos biflorus-FITC, a marker for the cyst wall. Cysts from each mouse brain homogenate were diluted and blindly counted in quadruplicate and back-

calculated to give the total number of cysts per brain (*circle* or *square* plots). The horizontal red lines represent the mean number of total brain cysts per cage of mice infected and error bars represent the standard deviation across diluted replicates for each brain (P = 0.13, student's *t* test).

Figure S6. Cas9-mediated disruption of GRA17, related to Figure 5.

Confluent HFFs were infected with *ΔGRA17/ΔGRA23+GRA17-HA* parasites that were transiently transformed with Cas9-3xFLAG and either non-specific or GRA17-specific gRNAs along with GRA17 donor oligonucleotide templates containing a nonsense mutation (described in Supplemental Experimental Procedures). The infected cells were fixed at 24 h and subjected to IF with anti-HA and anti-FLAG antibodies. The percentage of Cas9-3xFLAG-positive vacuoles and GRA17-HA-positive vacuoles out of the total were scored. This experiment was performed only once.

Figure S7. GRA17, GRA23, GRA15, and EXP2 expression in *Xenopus* oocytes, related to Figure 6.

(A) *Xenopus laevis* oocytes injected with 29 ng of *GRA17-HA* or 33 ng *GRA23-HA* cRNAs or mock injected for 3 days and snap-frozen. The oocytes were lysed and fractionated into total membrane and cytosol fractions as described in Supplementary Experimental Procedures. The lysates were subjected to SDS-PAGE and Western blotted with anti-HA and anti-GAPDH antibodies as indicated. **(B)** *Xenopus* oocytes were injected with 32 ng of *GRA15-HA* cRNA or mock injected for 3 days and fractionated into total membrane (M) or cytosol (C) fractions and Western blotted as in Fig. S7A. **(C)** *Xenopus* oocytes were injected with 29 ng of *GRA17-HA*, 33 ng of *GRA23-HA* cRNA, or equivalent volume water for 3 days and were snap-frozen, cryo-sectioned, fixed and processed by immunohistochemistry with anti-HA antibodies. Images were taken at 20× magnification using either phase-contrast brightfield (BF) or fluorescent deconvolution microscopy (scale bar = 50 μm). The oocyte membrane is indicated (*white arrows*) in

contrast to the background fluorescence of the pigment granules. **(D)** *Xenopus* oocytes were injected with 54 ng of *EXP2-HA* cRNA or mock injected for 3 days and fractionated into total membrane (M) or cytosol (C) fractions and Western blotted as in Fig. S7A. **(E)** Percent per condition survival of *Xenopus laevis* oocytes injected with 30 ng of *PfEXP2-HA* mRNA or equal volume H_2O, 3 days post-injection. Survival was based on a morphological appearance of the oocytes. Fractions on top of each bar graph represent the number of oocytes that survived out of the total injected for each condition. **(F)** Resting membrane potentials (RMP) of surviving oocytes injected with *PfEXP2-HA* cRNA or equal volume H_2O. **(G)** Average conductance (G) was computed by fitting the I-V relationship as a straight line. **(H)** Average membrane currents measured from a holding potential of -90 mV potentials of -120 mV to +50 mV were applied for 2 seconds. Peak currents from each applied voltage were used to generate an I-V relationship. For all above sub-figures, data are shown as the mean ±SE. Confidence levels were calculated using Student's paired t-test, where * signifies $P<0.05$ when compared to H_2O-injected oocytes.

Table S1. **DNA oligonucleotides used in this study, related to Figure 1.**

The name, sequence and brief description of each DNA oligonucleotide is presented in table form.

Table S2. **Genes uniquely up-regulated in the absence of GRA17, related to Figure 2.**

Analysis of the mRNA sequenced from the *Toxoplasma*-infected bone-marrow-derived macrophages in Fig. S3B. The data was filtered for genes expressed above an FPKM value threshold of 20 and containing strongly predicted signal peptides by SignalP 4.1. Relative expression was calculated by taking the binary logarithms of the ratio of FPKM values of either the *ΔGRA17* or *ΔGRA23* strains compared to the FPKM value the Wild-

type strain for each gene and filtered to include only those values ≥ 0.8 or ≤ 0.2, respectively. The ToxoDB.org gene identities, gene product names and values of the relative expression calculated above are listed in the table.

Videos S1 and S2. A subset of ∆*GRA17* PVs collapse and their tachyzoites become inviable over time, related to Figure 3.

Videos S1 and **S2** depict the same infected host cell as described in Figure 3A. Sub-confluent HFFs were infected with ∆*GRA17* tachyzoites. **Video S1** spans 19:30 h to 35:30 h post infection. Note the collapse of all but one PV in the host cell over this time course. **Video S2** spans a duration from 41:30 h to 62:00 h post-infection. Note the remaining PV contains dividing tachyzoites that eventually egress from the host cell but the tachyzoites in the collapsed PVs remain inviable. Images in both videos were collected every 30 minutes from a fixed field of view. Scale bars represent 10 µm.

Supplemental Videos 3 and 4. ∆*GRA17* enlarged PVs change shape and size dynamically and contain viable tachyzoites, related to Figure 3.

Videos S3 and **S4** depict the same infected host cell as described in Figure S5. Sub-confluent HFFs were infected with ∆*GRA17* tachyzoites. **Video S3** spans 21:30 h to 37:00 h post-infection. Note the dynamic growth of the PV, doubling of the number of tachyzoites and movement of the infected cell over this time course (imaged from a fixed point). **Video S4** spans a duration from 37:30 h to 51:30 h post-infection. Note the continued growth of the PV and the ultimate egress of the tachyzoites within it. Images in both videos were collected every 30 minutes; scale bars = 10 µm.

Table S2

Gene ID	Product Description	LOG_2 (ΔGRA17/WT)	LOG_2 (ΔGRA23/WT)
TGME49_278400	*T. gondii* family A protein	1.3	0.2
TGME49_319350	SAG-related sequence SRS17B	1.0	-0.2
TGME49_297880	GRA23	0.8	-5.9
TGME49_270170	hypothetical protein	0.8	0.2
TGME49_310610	hypothetical protein	0.8	-0.5
TGME49_222270	hypothetical protein	0.8	0.2

Supplemental experimental procedures

Antibodies

Rabbit polyclonal antibodies were raised against a synthetic C-terminal peptide derived from *Tg*GRA17 (CVPRLEALSAKMAVKQKAMQG) that was conjugated to keyhole limpet hemocyanin (KLH). The peptide synthesis, rabbit immunization and serum collection was conducted by Covance Research Products (Denver, PA). We used serum at a 1:1000 dilution for Western Blotting; this antibody fails to detect GRA17 by immunofluorescence (IF) microscopy. We used antibodies raised against HA (3F10, rat polyclonal, Roche, 1:500 for WB and IF; 1:100 for immunohistochemistry), FLAG (M2 mouse monoclonal, Sigma, 1:1000), GAPDH (6C5, mouse monoclonal, Santa Cruz, 1:750), V5 (mouse monoclonal, Life Technologies, 1:1000), *Toxoplasma* Surface Antigen (SAG)-1 (Burg et al., 1988) (DG52, purified mouse monoclonal, 1:5000 dilution for IF), *Tg*SAG1 (rabbit polyclonal, gift of J. Boothroyd, 1:5000 for Western Blotting or IF), *Tg*GRA4 (rabbit polyclonal, gift of L. Knoll, 1:2000), *Tg*GRA7 (Dunn et al., 2008) (rabbit polyclonal, gift of J. Boothroyd, 1:2000), *Tg*GRA1 (Charif et al., 1990), and *Tg*ROP1 (Ossorio et al., 1992). Secondary antibodies for IF were conjugated to Alexa-

488 and Alexa-594 (Life Technologies), and HRP-conjugated antibodies (Kirkegaard & Perry Laboratories) were used for Western Blotting.

Generation of transgenic, knockout, and complemented strains

We expressed *GRA17* (TGGT1_222170) as a transgene by amplifying its coding region with the primers TGGT1_222170_-1500_F and TGGT1_222170_HA_R (or TGGT1_222170_V5_R) containing the putative endogenous *GRA17* promoter from genomic DNA isolated from *Toxoplasma GT1* to clone into the pTKO-att vector that encodes GFP and the hypoxanthine-xanthine-guanine ribosyl transferase (HXGPRT) selectable marker using a Gateway (Life Technologies) cloning strategy described in (Rosowski et al., 2011). Electroporation, selection by mycophenolic acid/xanthine and cloning by limiting dilution were performed as previously described (Donald and Roos, 1998; Rosowski et al., 2011) into RH*ΔHXGPRT* and CEP*ΔHXGPRT* C22 (Boyle et al., 2007) (types I, II, and III respectively). To construct the vector pLIC-P_{GRA23}-*GRA23-HA-FLAG*, the promoter region of *GRA23* (TGGT1_297880) and *GRA23* coding sequence was amplified using the primers LIC_ TGGT1_297880_F and LIC_ TGGT1_297880_R from genomic DNA of the RH wild-type strain. The resulting PCR product was cloned into the pLIC-*HF-dhfr* vector using the LIC cloning method as described (Huynh and Carruthers, 2009) to generate the pLIC-*GRA23-HF-dhfr* plasmid.

We generated *GRA17* and *GRA23* knockouts with targeting constructs derived from the pTKO2 vector and Multisite Gateway Pro 3-Fragment Recombination (Life Technologies) strategy previously described (Rosowski et al., 2011) (Fig. S2A). Briefly, the 5' and 3' UTRs of *GRA17* or *GRA23* were engineered to flank the *HXGPRT* selectable marker in the pTKO2 plasmid. The fragment containing the *GRA17* 5'UTR was amplified with TGGT1_222170_5'UTR_attB1 and TGGT1_222170_5'UTR_attB4. The GRA17 3'UTR was amplified with TGGT1_222170_3'UTR_attB2 and TGGT1_222170_3'UTR_attB3. The fragment containing the *GRA23* 5'UTR was

amplified with primers TGGT1_297880_5'UTR_attB1 and TGGT1_297880_5'UTR_attB4. The GRA23 3'UTR was amplified with primers TGGT1_297880_3'UTR_attB3 and TGGT1_297880_3'UTR_attB2. An additional *GRA23* gene targeting construct was constructed using the above *GRA23* UTRs with a *DHFR-TS* selectable marker cassette (Donald and Roos, 1994). The *DHFR-TS* cassette was cloned into the Gateway pDONR 221 P4r-P3r vector by amplifying the cassette with the following forward and reverse primers: DHFR-TS_attB4r and DHFR-TS_attB3r. Electroporation, selection by mycophenolic acid/xanthine and cloning by limiting dilution were performed as described above into RH*ΔHXGPRT*/*ΔKu80* (Fox et al., 2009). The parasites were confirmed to contain gene knockouts by our ability to amplify the knockout construct and inability to amplify the coding region by PCR in these clones (Fig. S2A, B, and C). The RH*ΔGRA17* strain was complemented by disrupting the *Toxoplasma uracil phosphoribosyl transferase (UPRT)* locus with *GRA17-HA* or *Toxoplasma* codon-optimized *Plasmodium falciparum EXP2-HA* and positively selecting for the absence of UPRT with floxuridine (FUDR) (Bohne and Roos, 1997). The targeting construct was generated into pTKO2 using the approach outlined above, with the *GRA17-HA* transgene flanked by the 5' and 3' UTRs from *UPRT*. The *GRA17-HA* transgene was amplified from the cloned *GRA17* sequence contained in the pTKO-att plasmid described above using the TGGT1_222170_attB4r and TGGT1_222170_attB3r primers for cloning into pDONR221 P4r-P3r. The 5' and 3'UTRs of *UPRT* were amplified with the following forward and reverse primer pairs from isolated *Toxoplasma* RH genomic DNA: (5'UTR, forward: UPRT_5'UTR_attB1 and UPRT_5'UTR_attB4:; 3'UTR, forward: UPRT_5'UTR_attB3 and reverse: UPRT_5'UTR_attB2) for cloning into the pDONR221 P4-P1 and P3-P2, respectively. The chimeric *gra1*-5'UTR-*GRA23-HA-FLAG* transgene was generated by a 2-step "sewing PCR" where the *gra1* 5'UTR fragment (#1) was PCR amplified with the gra1_5'UTR_attB4r and gra1_5'UTR_GRA23bridge_R

primers from a RH-derived genomic DNA template such that it contains a 3' extension of *GRA23* coding sequence. A *GRA23-HA-FLAG* coding sequence fragment (#2) was generated by PCR amplification using the gra1_5'UTR_GRA23bridge_F and DHFR-TS_attB3r with the pLIC-*GRA23-HF-dhfr* plasmid as template. Fragment #2 contains a 5'extension containing *gra1* 5'UTR sequence that overlaps with the first fragment, enabling a second round of PCR amplification using the gra1_5'UTR_attB4r and DHFR-TS_attB3r primers and fragments #1 and #2 as templates to generate the chimeric *gra1*-5'UTR-*GRA23-HF-dhfr* sequence to combine with the *UPRT* flanking sequences as described above.

Endogenous tagging of *Toxoplasma* GRA24 was performed by digesting the pLIC-P_{GRA1}-*GRA24-HA-FLAG* (Braun et al., 2013) plasmid DNA with a restriction endonuclease within the coding sequence and transforming the target strains as previously described (Huynh and Carruthers, 2009).

The *Plasmodium falciparum EXP2* cDNA was codon optimized for *E. coli* by DNA 2.0 (Menlo Park, CA) using proprietary parameters that optimize expression by codon usage as well as RNA stability using secondary structure predictions. The resulting *EXP2* cDNA (below) was PCR amplified, adding an HA tag to the C-terminus with EXP2_NsiI_F and EXP2_PacI_R primers and cloned into the p*GRAGFP/HPT* plasmid (Rome et al., 2008) in which *GFP* was removed and the *EXP2-HA* coding sequence added using *NsiI* and *PacI* restriction sites.

This *PfEXP2-HA* expression cassette was then amplified with the following forward and reverse primers for Gateway cloning into the pDONR 221 P4r-3r: EXP2_attB4r and EXP2_attB3r. *Toxoplasma*-codon optimized *PfEXP2* coding sequence:

5'atgcatAAAGTTAGCTACATCTTTAGCTTCTTCTTGCTGTTCTTCGTCTACAAGAACAC
GAATACCGTCGTTTGCGACAATGGTTACGGTGACTTGGCTGCGACCTCCGCGTTGA
CGACGGTTATCAAAGATCCGATTTCCCTGACGATTAAGGACATTTACGAGCACGGT

GTGAAGAATCCGTTTACCAAGATCATTCATAAACTGAAGAAGTTTATCCGCTATCGC
AAAGTTCTGCGTTGGTCGCGTATGTGGTGGGTCCTGCTGGTTCGCGAGATCGTCG
GTGACAATACGATTGAGAAAAAGACCGAGAAAGCGCTGCGTGAAATCTGGGATCAA
TGCACCATCGCGGTGTATAACAACACCCTGAACGCGGTGGAAAGCAAGCCGCTGC
TGTTCCTGCATGGTATTCTGAACGAGTGTCGCAACAACTTCGCCACCAAACTGCGT
CAGGACCCGAGCCTGATTGTCGCCAAGATCGACCAGATTATCAAAAGCCAGATTTA
CCGTTTTTGGGTGAGCGAGCCGTATCTGAAAATCGGCCGTAGCCATACCCTGTATA
CGCACATCACTCCGGATGCAGTGCCACAATTGCCTAAAGAATGTACTCTGAAACAC
CTGAGCAGCTACATGGAAGAGAAGCTGAAGTCTATGGAATCGAAGAAAAACATTGA
ATCCGGTAAGTATGAGTTCGATGTTGATTCCAGCGAAACCGATAGCACCAAAGACG
ACGGTAAGCCGGATGACGATGATGACGACGACGATAACTTTGACGACGATGACAAT
TTCGATGATGATACGGTTGAAGAAGAGGACGCATCTGGCGACCTGTTTAAGAATGA
GAAGAAAGACGAAAATAAGGAA3’

Design and cloning of guide RNA for Cas9-mediated gene disruption

The GRA17gRNA_L32stop+ and GRA17gRNA_L32stop- oligonucleotides encoding a target sequence within *GRA17* were annealed and ligated into the guide RNA (gRNA) expression cassette in a *BsaI*-digested pSS013 vector (Sidik et al., 2014), also encoding *Cas9-3xFLAG*. The GRA17donor_L32stop+ and GRA17donor_L32stop- oligonucleotides were annealed for co-electroporation with the pSS013 vector to serve as a template for homologous recombination. As above, the following oligos were used to create gDNA/oligonucleotide donor template combinations: Gly20stop [gRNA oligos: GRA17gRNA_G20stop+ and GRA17gRNA_G20stop-; donor template oligos: GRA17donor_G20stop+ and GRA17donor_G20stop-]; Lys54stop [gRNA oligos: GRA17gRNA_K54stop+ and GRA17gRNA_K54stop-; donor templates: GRA17donor_K54stop+ and GRA17donor_K54stop-].

Western blotting and immunofluoresence

Infected HFFs were lysed and samples were prepared for Western blotting as described (Rosowski et al., 2011). Extracellular parasites were derived from cells that were newly lysed out and washed 3× with PBS and lysed for Western blotting as above. IF was performed as previously described (Rosowski et al., 2011).

Extracellular tachyzoite staining

Extracellular parasites were derived from cells that were freshly lysed out and washed 3× with PBS, centrifuged onto coverslips at 163 × g for 3 minutes and subjected to IF.

RNA sequencing

Bone marrow-derived mouse macrophages were isolated and infected as previously described (Hassan et al., 2012). Total RNA excluding miRNA was extracted with the Qiagen RNeasy Plus kit (Qiagen, USA) and assayed for integrity, size distribution and concentration with the Agilent 2100 Bioanalyser. The mRNA was isolated with the Dynabead mRNA purification kit (Invitrogen) and processed for sequencing on an Illumina HiSeq 2000 machine according to standard Illumina protocols. The sequences were assembled and aligned to the ME49 8.0 genome as previously described (Hassan et al., 2012). The accession number for the mRNA sequencing data reported in this paper is GEO: GSE65980.

***In vivo* mouse imaging and physiology**

5 female BALB/c (age 6 weeks, The Jackson Laboratory) were infected intraperitoneally with 10,000 tachyzoites and imaged *in vivo* as described previously (Rosowski et al., 2011). Brain homogenate of chronically infected mice was stained with dolichos biflorus-FITC (Vector Laboratories), and cysts were enumerated by microscopy. For all infections, plaque assays were performed after the experiment to assess relative parasite MOI and found to yield an equivalent number of plaques across strains per experiment and all surviving mice were verified to be seropositive for *Toxoplasma* antigen. Mice determined to be below a body condition score of 2 were euthanized and

counted as dead in accordance with institutional and federal regulations. All mice were maintained in specific pathogen-free conditions. The MIT Committee on Animal Care approved all protocols (assurance number A-3125-01).

Cloning and preparation of cRNA for *Xenopus* oocyte injection

To clone cDNAs of *GRA17*, *GRA23*, and $GRA15_{II}$, total RNA was isolated from infected cells and a cDNA pool was created as described (Rosowski et al., 2011) and PCR-amplified with the following forward and reverse primers, respectively (*GRA17*: GRA17_-SigP_BamHI_F and GRA17_NotI_R or GRA17_HA_NotI_R; *GRA23*: GRA23_-SigP_BamHI_F and GRA23_NotI_R or GRA23_HA_NotI_R; *GRA15*: GRA15_-SigP_BamHI_F and GRA15_SpeI_R or GRA15_HA_SpeI_R; *EXP2*: EXP2_-SigP_BamHI_F and EXP2_NotI_R or EXP2_HA_NotI_R) for ligation into pBluescript KS+ with *BamHI* and *NotI* restriction sites for *GRA17*, *GRA23*, and *EXP2* and BamHI and *SpeI* restriction sites for *GRA15*. The start sites for each cDNA were chosen immediately after the predicted signal peptide cleavage site and a heterologous Kozak sequence and start codon were added to the upstream primers. An additional heterologous glycine residue was added after the start codon of the *GRA15* cDNA for stability. The plasmids were digested with PvuI endonuclease and cRNA was generated and prepared for oocyte injection as described (Bett et al., 2012).

Isolation of total membranes and cytosol from *Xenopus* oocytes

As described in (Engelund et al., 2013; Kamsteeg and Deen, 2001) injected oocytes (~12 oocytes per tube) were mechanically lysed with a p200 pipette tip in HbA buffer [20 mM Tris-HCl (pH7.4), 5 mM MgCl2, 5 mM NaH2PO4, 1 mM EDTA, 80 mM sucrose and 25× of a protease inhibitor cocktail (Cat# 04693116001, Roche)]. The lysates were centrifuged at 200 × g at 4 °C for 5 minutes and the resulting supernatant was taken and centrifuged at 20,000 × g at 4 °C for 20 minutes. The supernatant (cytosolic fraction) and

the pellet (the total membrane fraction) were separated and treated with 2× Laemmli Sample Buffer, boiled, and subjected to SDS-PAGE and Western blotting.

Xenopus oocytes immunohistochemistry

cRNA-injected *Xenopus* oocytes were snap frozen unfixed in OCT freezing media. The blocks were cryo-sectioned into 6 µm slices onto glass slides. The slides were then fixed with 4% paraformaldehyde for 15 minutes at room temperature. The slides were washed 2× with PBS and then incubated with 0.25% Triton X-100 in PBS for 10 minutes. The slides were washed 3× with PBS and blocked for 1 hour in IHC Blocking Buffer (IHC-BB) [1 mg/ml Blocking Reagent (Perkin Elmer, Cat# FP1012), 2% heat-inactivated goat serum, in 0.1 M Tris, pH 7.5, and 0.15 M NaCl]. The slides were incubated with primary antibody diluted in IHC-BB overnight at 4 °C and subsequently washed 3× with PBS. The slides were incubated with goat anti-rat Alexa-594 (Life Technologies) secondary antibody diluted 1:500 in IHC-BB for 1 hour at room temperature. The slides were washed 3× with PBS and mounted for imaging.

Supplemental References

Bawono, P., and Heringa, J. (2014). PRALINE: a versatile multiple sequence alignment toolkit. Methods Mol. Biol. *1079*, 245–262.

Bett, G.C.L., Lis, A., Guo, H., Liu, M., Zhou, Q., and Rasmusson, R.L. (2012). Interaction of the S6 proline hinge with N-type and C-type inactivation in Kv1.4 channels. Biophys. J. *103*, 1440–1450.

Bohne, W., and Roos, D.S. (1997). Stage-specific expression of a selectable marker in *Toxoplasma gondii* permits selective inhibition of either tachyzoites or bradyzoites. Mol Biochem Parasitol *88*, 115–126.

Boyle, J.P., Saeij, J.P., and Boothroyd, J.C. (2007). *Toxoplasma gondii*: inconsistent dissemination patterns following oral infection in mice. Exp Parasitol *116*, 302–305.

Braun, L., Brenier-Pinchart, M.P., Yogavel, M., Curt-Varesano, A., Curt-Bertini, R.L., Hussain, T., Kieffer-Jaquinod, S., Coute, Y., Pelloux, H., Tardieux, I., et al. (2013). A *Toxoplasma* dense granule protein, GRA24, modulates the early immune response to

infection by promoting a direct and sustained host p38 MAPK activation. J Exp Med *210*, 2071–2086.

Burg, J.L., Perelman, D., Kasper, L.H., Ware, P.L., and Boothroyd, J.C. (1988). Molecular analysis of the gene encoding the major surface antigen of *Toxoplasma gondii*. J Immunol *141*, 3584–3591.

Charif, H., Darcy, F., Torpier, G., Cesbron-Delauw, M.F., and Capron, A. (1990). *Toxoplasma gondii*: characterization and localization of antigens secreted from tachyzoites. Exp Parasitol *71*, 114–124.

Donald, R.G., and Roos, D.S. (1994). Homologous recombination and gene replacement at the dihydrofolate reductase-thymidylate synthase locus in *Toxoplasma gondii*. Mol Biochem Parasitol *63*, 243–253.

Donald, R.G., and Roos, D.S. (1998). Gene knock-outs and allelic replacements in *Toxoplasma gondii*: HXGPRT as a selectable marker for hit-and-run mutagenesis. Mol Biochem Parasitol *91*, 295–305.

Dunn, J.D., Ravindran, S., Kim, S.K., and Boothroyd, J.C. (2008). The *Toxoplasma gondii* dense granule protein GRA7 is phosphorylated upon invasion and forms an unexpected association with the rhoptry proteins ROP2 and ROP4. Infect Immun *76*, 5853–5861.

Engelund, M.B., Chauvigné, F., Christensen, B.M., Finn, R.N., Cerdà, J., and Madsen, S.S. (2013). Differential expression and novel permeability properties of three aquaporin 8 paralogs from seawater-challenged Atlantic salmon smolts. J. Exp. Biol. *216*, 3873–3885.

Fox, B.A., Ristuccia, J.G., Gigley, J.P., and Bzik, D.J. (2009). Efficient gene replacements in *Toxoplasma gondii* strains deficient for nonhomologous end joining. Eukaryot Cell *8*, 520–529.

Hassan, M.A., Melo, M.B., Haas, B., Jensen, K.D., and Saeij, J.P. (2012). De novo reconstruction of the *Toxoplasma gondii* transcriptome improves on the current genome annotation and reveals alternatively spliced transcripts and putative long non-coding RNAs. BMC Genomics *13*, 696.

Huynh, M.H., and Carruthers, V.B. (2009). Tagging of endogenous genes in a *Toxoplasma gondii* strain lacking Ku80. Eukaryot Cell *8*, 530–539.

Kamsteeg, E.J., and Deen, P.M. (2001). Detection of aquaporin-2 in the plasma membranes of oocytes: a novel isolation method with improved yield and purity. Biochem. Biophys. Res. Commun. *282*, 683–690.

Ossorio, P.N., Schwartzman, J.D., and Boothroyd, J.C. (1992). A *Toxoplasma gondii* rhoptry protein associated with host cell penetration has unusual charge asymmetry. Mol Biochem Parasitol *50*, 1–15.

Rome, M.E., Beck, J.R., Turetzky, J.M., Webster, P., and Bradley, P.J. (2008). Intervacuolar transport and unique topology of GRA14, a novel dense granule protein in *Toxoplasma gondii*. Infect Immun *76*, 4865–4875.

Rosowski, E.E., Lu, D., Julien, L., Rodda, L., Gaiser, R.A., Jensen, K.D., and Saeij, J.P. (2011). Strain-specific activation of the NF-kappaB pathway by GRA15, a novel *Toxoplasma gondii* dense granule protein. J Exp Med *208*, 195–212.

Sidik, S.M., Hackett, C.G., Tran, F., Westwood, N.J., and Lourido, S. (2014). Efficient Genome Engineering of *Toxoplasma gondii* Using CRISPR/Cas9. PLoS One *9*, e100450.

Tamura, K., Peterson, D., Peterson, N., Stecher, G., Nei, M., and Kumar, S. (2011). MEGA5: molecular evolutionary genetics analysis using maximum likelihood, evolutionary distance, and maximum parsimony methods. Mol. Biol. Evol. *28*, 2731–2739.